# Design of the Symmetrical OTA

Version 1

Christian Enz

2025 - 05 - 08

# Table of contents

1	Intro	oduction											
2	Ana	Analysis											
	2.1	Small-signal analysis											
	2.2	Noise analysis											
		2.2.1 Input-referred thermal noise											
		2.2.2 Input-referred flicker noise											
	2.3	Input-referred offset voltage											
3	Desi	Design 1											
	3.1	Specifications											
	3.2	Process											
	3.3	Design procedure											
	0.0	3.3.1 Sizing the differential pair $M_{1a}$ - $M_{1b}$											
		3.3.2 Sizing the pMOS current mirrors $M_{2a}$ - $M_{2c}$ and $M_{2b}$ - $M_{2d}$											
		3.3.3 Sizing the nMOS current mirror $M_{3a}$ and $M_{3b}$											
		3.3.4 Sizing the cascode transistors $M_4$ - $M_7$											
		3.3.5 Sizing the nMOS current mirror $M_{5a}$ - $M_{5b}$											
		3.3.6 Final sizing of the differential pair $M_{1a}$ - $M_{1b}$											
	3.4	Summary											
	0.1	3.4.1 Specifications											
		3.4.2 Bias											
		3.4.3 Transistor information											
		5.4.9 Itansistoi information											
1	OTA	A Characteristics											
	4.1	Open-loop gain											
	4.2	Input-referred noise											
	4.3	Input-referred offset voltage											
	4.4	Current and power consumption											
5	Sim	ulation results from ngspice											
	5.1	Operating point											
	5.2	Large-signal differential transfer characteristic											
	5.3	Open-loop gain											
		5.3.1 Closed-loop circuit											
		5.3.2 Open-loop circuit											
	5.4	Input-referred noise											
	5.5	Input common-mode voltage range											
	5.6	Step-response											
		5.6.1 Small-step											
		5.6.2 Large step											
	5.7	Current and power consumption											
_													
6	Con	clusion											
Re	feren	nces											

## 1 Introduction

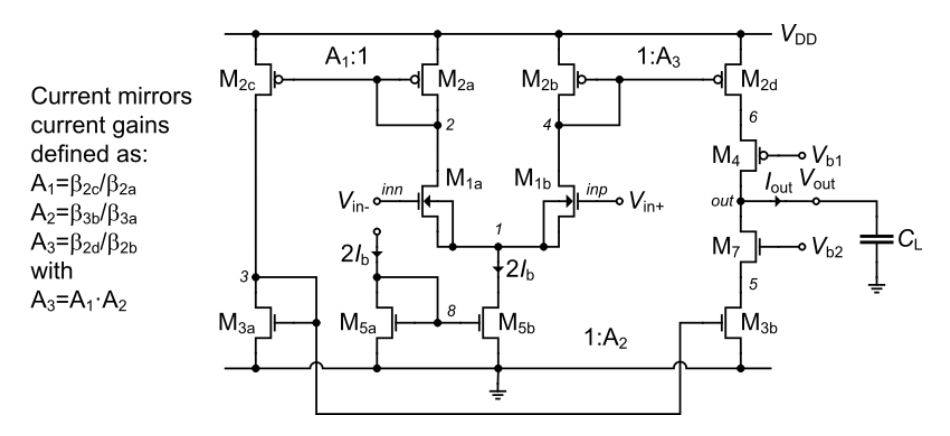


Figure 1.1: Schematic of the symmetrical differential OTA.

#### Note

Note that all nMOS transistors in Figure 1.1 have an odd number and all the pMOS transistors an even number which explains the numbering process (this is the reason why there is no  $M_6$  transistor!).

This notebook presents the analysis, design and simulation of the symmetrical cascode OTA which schematic is presented in Figure 1.1 [1]. The design phase is using the sEKV model and the inversion coefficient approach [2], [3], [4]. The symmetrical OTA is a single-stage OTA having the dominant pole set by the load capacitance. It therefore doesn't require any compensation capacitance but can still achieve the gain of a two-stage OTA thanks to the cascode stages at the output at much lower current consumption. We will see below that in differential mode the effects of the source transconductances on the common source node voltage are actually canceled. In order to minimize the  $V_{GS}$  voltage of  $M_{1a}$ - $M_{1b}$ , we have chosen to put  $M_{1a}$ - $M_{1b}$  in a separate well at the cost of a larger area.

We will start with a detailed analysis of the OTA which will allow to derive all the design equations that will be used in the design phase. The OTA is then designed for a given set of specifications for the chosen IHP SG13G2 130nm BiCMOS technology [5]. We have selected this technology because IHP provides an open source PDK which is then used for the validation of the design by simulation with ngspice [6] using the PSP compact model [7] provided by the open source PDK [5].

## 2 Analysis

#### 2.1 Small-signal analysis

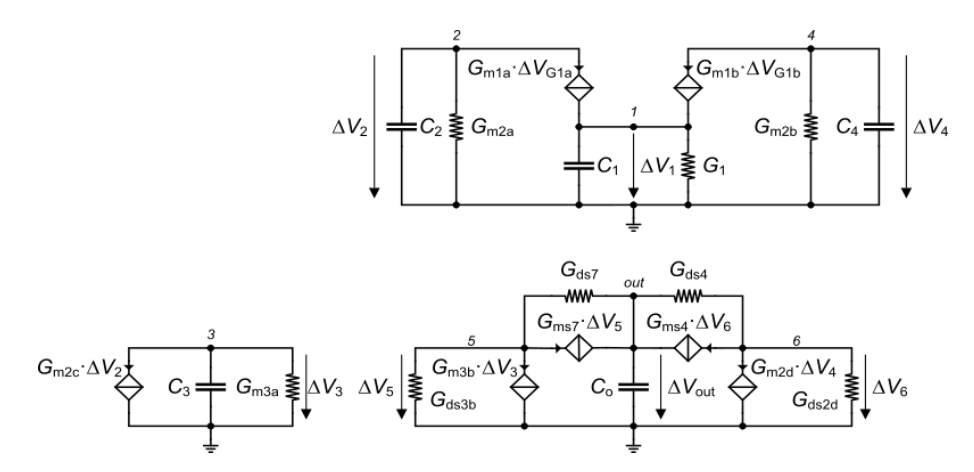


Figure 2.1: Small-signal schematic of the symmetrical cascode OTA.

We start with the small-signal analysis. The small-signal schematic of the symmetrical OTA of Figure 1.1 is shown in Figure 2.1. The design of the symmetrical cascode OTA is similar to the design of the simple OTA, except that there are now more parasitic poles appearing at the various current mirror nodes. The small-signal output voltage in open-loop is given by

$$\Delta V_{out} = \frac{A_{dc}}{1 + s \,\tau_0} \cdot \left[ \frac{\Delta V_{in+}}{1 + s \,\tau_{p4}} - \frac{\Delta V_{in-}}{(1 + s \,\tau_{p2})(1 + s \,\tau_{p3})} \right]$$
(2.1)

$$-\frac{\Delta V_{in+} + \Delta V_{in-}}{2(1+s\,\tau_{p1})} \cdot \left(\frac{1}{1+s\,\tau_{p4}} - \frac{1}{(1+s\,\tau_{p2})(1+s\,\tau_{p3})}\right)$$
 (2.2)

where

$$A_{dc} = \frac{G_m}{G_o},\tag{2.3}$$

$$G_m = A_3 \cdot G_{m1},\tag{2.4}$$

$$G_{m} = A_{3} \cdot G_{m1}, \qquad (2.4)$$

$$G_{o} = \frac{G_{ds3b} G_{ds7}}{G_{ms7}} + \frac{G_{ds2d} G_{ds4}}{G_{ms4}}, \qquad (2.5)$$

$$\tau_{0} = \frac{C_{out}}{G_{o}}, \qquad (2.6)$$

$$\tau_0 = \frac{C_{out}}{G_o},\tag{2.6}$$

$$C_{out} = C_o + C_L, (2.7)$$

$$\tau_{p1} = \frac{C_1}{2G_{m1}},\tag{2.8}$$

$$\tau_{p2} = \frac{C_2}{G_{m2}},\tag{2.9}$$

$$\tau_{p3} = \frac{C_3}{G_{m3}},\tag{2.10}$$

$$\tau_{p4} = \frac{C_4}{G_{m2}}. (2.11)$$

The unity-gain frequency or gain-bandwidth product is defined as  $\omega_u = 1/\tau_u \triangleq A_{dc}/\tau_0 = G_m/C_{out}$ . In most practical cases, we usually have  $\tau_0 \gg \tau_{p2}, \tau_{p3}, \tau_{p4} > \tau_{p1}$ .

For a differential input voltage  $\Delta V_{id} = \Delta V_{in+} - \Delta V_{in-}$  with a constant common-mode voltage  $V_{ic}$  and hence  $\Delta V_{ic} = (\Delta V_{in+} + \Delta V_{in-})/2 = 0$ ,  $\Delta V_{in+} = \Delta V_{in-} = \Delta V_{id}/2$ , the differential mode small-signal open-loop gain reduces to

$$A_{dm}(s) \triangleq \frac{\Delta V_{out}}{\Delta V_{id}} = \frac{1}{2} \cdot \frac{A_{dc}}{1 + s \tau_0} \cdot \left[ \frac{1}{1 + s \tau_{p4}} - \frac{1}{(1 + s \tau_{p2})(1 + s \tau_{p3})} \right]. \tag{2.12}$$

The small-signal output voltage  $\Delta V_{out}$  can also be written as

$$\Delta V_{out} = \frac{A_{dc}}{1 + s \tau_0} \cdot \left[ F(s) \cdot \Delta V_{in+} - G(s) \cdot \Delta V_{in-} \right], \qquad (2.13)$$

where

$$F(s) = \frac{1}{1+s\,\tau_{p4}} - \frac{1}{2}\,\frac{1}{1+s\,\tau_{p1}} \cdot \left[ \frac{1}{1+s\,\tau_{p4}} - \frac{1}{(1+s\,\tau_{p2})(1+s\,\tau_{p3})} \right],\tag{2.14}$$

$$G(s) = \frac{1}{(1+s\,\tau_{p2})(1+s\,\tau_{p3})} + \frac{1}{2}\,\frac{1}{1+s\,\tau_{p1}} \cdot \left[\frac{1}{1+s\,\tau_{p4}} - \frac{1}{(1+s\,\tau_{p2})(1+s\,\tau_{p3})}\right]. \tag{2.15}$$

From (2.13) we see that the time constant  $\tau_0$  introduces a  $-90^{\circ}$  phase shift. Hence if the desired phase margin is at least 60°, the additional phase shift introduced by the smaller time constants  $\tau_{p1}$ ,  $\tau_{p2}$ ,  $\tau_{p3}$  and  $\tau_{p4}$  should not exceed 30°. In this range, the product  $(1 + s \tau_{p1})(1 + s \tau_{p2})(1 + s \tau_{p3})(1 + s \tau_{p4})$  can be expanded and approximated by neglecting all the order terms higher than the first order term in s

$$\prod_{k=1}^{4} (1 + s \, \tau_{pk}) \cong 1 + s \, \sum_{k=1}^{4} \tau_{pk}. \tag{2.16}$$

The above approximation gives a good estimation of the phase shift  $\phi$  for  $\phi < 30^{\circ}$ , which correspond to the following frequency range

$$\omega \le \left(2\sum_{k=1}^4 \tau_{pk}\right)^{-1}.\tag{2.17}$$

Using the above approximation leads to

$$F(s) \cong G(s) \cong \frac{1 + s \tau_n}{1 + s \tau_d},\tag{2.18}$$

where

$$\tau_n = \tau_{p1} + \frac{\tau_{p2} + \tau_{p3} + \tau_{p4}}{2},\tag{2.19}$$

$$\tau_d = \tau_{p1} + \tau_{p2} + \tau_{p3} + \tau_{p4}. \tag{2.20}$$

For  $\omega \leq 1/(2\tau_d)$ , the above expression can be further simplified considering that

$$\frac{1+s\,\tau_n}{1+s\,\tau_d} \cong \frac{1}{1+s\,(\tau_d-\tau_n)} \tag{2.21}$$

where

$$\tau_d - \tau_n = \frac{\tau_{p2} + \tau_{p3} + \tau_{p4}}{2} = \frac{\tau_p}{2}.$$
 (2.22)

F(s) and G(s) become

$$F(s) \cong G(s) \cong \frac{1}{1 + s\frac{\tau_p}{2}},\tag{2.23}$$

which is valid for  $\omega \leq 1/(2\tau_d) = 1/(2(\tau_{p2} + \tau_p))$ .

The simplified differential transfer function is then given by

$$A_{dm}(s) \cong \frac{A_{dc}}{\left(1 + s\,\tau_0\right)\left(1 + s\,\frac{\tau_p}{2}\right)} = \frac{A_{dc}}{\left(1 + \frac{s}{\omega_0}\right)\left(1 + \frac{s}{\omega_p}\right)} \tag{2.24}$$

with  $\omega_0 \triangleq 1/\tau_0$  and  $\omega_p \triangleq 2/\tau_p$  where it is assumed that  $\tau_p = \tau_{p2} + \tau_{p3} + \tau_{p4} \ll \tau_0$ .  $\omega_0 \triangleq 1/\tau_0 \ll \omega_p$  is the dominant pole which is set by the load capacitance at the OTA output, whereas  $\omega_p \triangleq 2/\tau_p$  represents the non-dominant pole related to all the time constants due to the parasitic capacitances at the current mirror nodes.

The transfer function can be further simplified as

$$A_{dm}(s) \cong \frac{1}{s \tau_u \left(1 + s \frac{\tau_p}{2}\right)} = \frac{1}{\frac{s}{\omega_u} \left(1 + \frac{s}{\omega_p}\right)}$$
 (2.25)

where  $\omega_u = 1/\tau_u = A_{dc} \cdot \omega_0 = G_m/C_{out}$  is the unity gain frequency or the gain-bandwidth product GBW which is set by the OTA transconductance  $G_m$  and the load capacitance  $C_{out}$ .

#### 2.2 Noise analysis

We have seen that the noise of the cascode transistors  $M_4$  and  $M_7$  can actually be neglected. Remembering that  $A_3 = A_1 \cdot A_2$ , the PSD of the output noise current is given by

$$S_{I_{nout}} = A_3^2 \left( S_{I_{n1a}} + S_{I_{n1b}} + S_{I_{n2a}} + S_{I_{n2b}} \right) + A_2^2 \left( S_{I_{n2c}} + S_{I_{n3a}} \right) + S_{I_{n2d}} + S_{I_{n3b}}$$
 (2.26)

or if we express the output PSD in terms of the output noise conductance

$$S_{I_{nout}} = 4kT \cdot G_{nout} \tag{2.27}$$

where

$$G_{nout} = 2A_3^2 \cdot (G_{n1} + G_{n2}) + A_2^2 \cdot (G_{n2c} + G_{n3a}) + G_{n2d} + G_{n3b}$$
(2.28)

where we have assumed that  $M_{1a}$  and  $M_{1b}$  and  $M_{2a}$  and  $M_{2b}$  are identical. The  $G_{ni}$  are given by

$$G_{ni} = \gamma_{ni} \cdot G_{mi} + G_{mi}^2 \cdot \frac{\rho_i}{W_i L_i f} \qquad \text{for all transistors.}$$
 (2.29)

The input-referred noise resistance  $R_{nin}$  is then given by

$$R_{nin} \triangleq \frac{G_{nout}}{A_3^2 \cdot G_{m1}^2} = \frac{2(G_{n1} + G_{n2})}{G_{m1}^2} + \frac{G_{n2c} + G_{n3a}}{A_1^2 \cdot G_{m1}^2} + \frac{G_{n2d} + G_{n3b}}{A_3^2 \cdot G_{m1}^2}$$
(2.30)

where we have used  $A_3 = A_1 \cdot A_2$ . As expected, we see that the noise contribution to the input-referred noise of  $M_{2d}$  and  $M_{3b}$  is divided by  $A_3^2$  and that from  $M_{2c}$  and  $M_{3a}$  is divided by  $A_1^2$ .

We now look at the input-referred thermal and flicker noise separately.

#### 2.2.1 Input-referred thermal noise

The input-referred thermal noise resistance is given by

$$R_{nth} = \frac{2\gamma_{n1}}{G_{m1}} \cdot (1 + \eta_{th}) \tag{2.31}$$

where

$$\eta_{th} = \frac{\gamma_{n2}}{\gamma_{n1}} \frac{G_{m2}}{G_{m1}} + \frac{1}{2A_1^2} \left( \frac{\gamma_{n2c}}{\gamma_{n1}} \frac{G_{m2c}}{G_{m1}} + \frac{\gamma_{n3a}}{\gamma_{n1}} \frac{G_{m3a}}{G_{m1}} \right) + \frac{1}{2A_3^2} \left( \frac{\gamma_{n2d}}{\gamma_{n1}} \frac{G_{m2d}}{G_{m1}} + \frac{\gamma_{n3b}}{\gamma_{n1}} \frac{G_{m3b}}{G_{m1}} \right)$$
(2.32)

represents the contributions to the input-referred thermal noise of the current mirrors relative to that of the differential pair. Now  $G_{m2c} = A_1 \cdot G_{m2a} = A_1 \cdot G_{m2}$ ,  $G_{m3b} = A_2 \cdot G_{m3a} = A_2 \cdot G_{m3}$  and  $G_{m2d} = A_3 \cdot G_{m2b} = A_3 \cdot G_{m2}$ , and assuming that  $\gamma_{n2a} = \gamma_{n2b} \cong \gamma_{n2c} \cong \gamma_{n2d} = \gamma_{n2}$  and  $\gamma_{n3a} \cong \gamma_{n3b} = \gamma_{n3}$ , then  $\eta_{th}$  reduces to

$$\eta_{th} = \frac{\gamma_{n2}}{2\gamma_{n1}} \frac{G_{m2}}{G_{m1}} \left( 2 + \frac{1}{A_1} + \frac{1}{A_3} \right) + \frac{1}{2A_1^2} \frac{\gamma_{n3}}{\gamma_{n1}} \frac{G_{m3}}{G_{m1}} \left( 1 + \frac{1}{A_2} \right)$$
(2.33)

In the case of unity current gains  $A_1 = A_2 = A_3 = 1$ ,  $\eta_{th}$  simplifies further to

$$\eta_{th} = 2\frac{\gamma_{n2}}{\gamma_{n1}} \frac{G_{m2}}{G_{m1}} + \frac{\gamma_{n3}}{\gamma_{n1}} \frac{G_{m3}}{G_{m1}}$$
(2.34)

Of course in the design process, we will try to minimize  $\eta_{th}$  so that the dominant contribution to the input-referred thermal noise comes from the differential pair  $M_{1a}$ - $M_{1b}$ .

We can also introduce the OTA thermal noise excess factor as

$$\gamma_{ota} \triangleq G_m \cdot R_{nth}, \tag{2.35}$$

where  $G_m = A_3 \cdot G_{m1}$  is the OTA transconductance. This results in

$$\gamma_{ota} = 2A_3 \cdot \gamma_{n1} \cdot (1 + \eta_{th}). \tag{2.36}$$

We see that introducing some current gains larger than one in the current mirrors allows to reduce the contributions of transistors  $M_{2c}$ - $M_{2d}$  and  $M_{3a}$ - $M_{3b}$ , but on the other hand increases the contribution of the differential pair and hence degrading (i.e. increasing) the OTA thermal noise excess factor  $\gamma_{ota}$ .

For  $G_{m1} \gg G_{m2}$  and  $G_{m1} \gg G_{m3}$ , the noise is dominated by the differential pair and

$$\gamma_{ota} \cong 2A_3 \cdot \gamma_{n1}. \tag{2.37}$$

For unity current gains  $A_1 = A_2 = A_3 = 1$ , the OTA thermal noise excess factor  $\gamma_{ota}$  reduces to

$$\gamma_{ota} \cong 2\gamma_{n1}. \tag{2.38}$$

#### 2.2.2 Input-referred flicker noise

The input-referred flicker noise resistance is given by

$$f \cdot R_{nfl} = \frac{2\rho_n}{W_1 L_1} + \rho_p \left(\frac{G_{m2}}{G_{m1}}\right)^2 \left(\frac{2}{W_2 L_2} + \frac{1}{W_{2c} L_{2c}} + \frac{1}{W_{2d} L_{2d}}\right) \tag{2.39}$$

$$+\frac{\rho_n}{A_1^2} \left(\frac{G_{m3}}{G_{m1}}\right)^2 \left(\frac{1}{W_{3a}L_{3a}} + \frac{1}{W_{3b}L_{3b}}\right) \tag{2.40}$$

which can be written as

$$R_{nfl} = \frac{2\rho_n}{W_1 L_1 f} \cdot (1 + \eta_{fl}) \tag{2.41}$$

where  $\eta_{fl}$  represents the contributions to the input-referred flicker noise resistance of the current mirrors relative to that of the differential pair

$$\eta_{fl} = \frac{\rho_p}{2\rho_n} \left(\frac{G_{m2}}{G_{m1}}\right)^2 \left(\frac{2W_1L_1}{W_2L_2} + \frac{W_1L_1}{W_{2c}L_{2c}} + \frac{W_1L_1}{W_{2d}L_{2d}}\right) \tag{2.42}$$

$$+\frac{1}{2A_1^2} \left(\frac{G_{m3}}{G_{m1}}\right)^2 \left(\frac{W_1 L_1}{W_{3a} L_{3a}} + \frac{W_1 L_1}{W_{3b} L_{3b}}\right). \tag{2.43}$$

For  $A_1 = A_2 = A_3 = 1$ ,  $W_{2a} = W_{2b} = W_{2c} = W_{2d} = W_2$ ,  $L_{2a} = L_{2b} = L_{2c} = L_{2d} = L_2$ ,  $W_{3a} = W_{3b} = W_3$  and  $L_{3a} = L_{3b} = L_3$  reduces to

$$\eta_{fl} = 2\frac{\rho_p}{\rho_n} \left(\frac{G_{m2}}{G_{m1}}\right)^2 \frac{W_1 L_1}{W_2 L_2} + \left(\frac{G_{m3}}{G_{m1}}\right)^2 \frac{W_1 L_1}{W_3 L_3}.$$
 (2.44)

Similarly to thermal noise, in the design process we will try to minimize  $\eta_{fl}$  in order to reduce the input-referred flicker noise to the contribution of the differential pair  $M_{1a}$ - $M_{1b}$ .

The corner frequency is obtained by equating  $R_{nfl(f_k)} = R_{nth}$  resulting in

$$f_k = \frac{\rho_n G_{m1}}{W_1 L_1 \gamma_{n1}} \cdot \frac{1 + \eta_{fl}}{1 + \eta_{th}}.$$
 (2.45)

#### 2.3 Input-referred offset voltage

The input-referred random offset voltage can be obtained in a similar way than noise. The variance of the input-referred offset voltage is given by

$$\sigma_{V_{os}}^2 = \sigma_{V_{T_1}}^2 \cdot (1 + \xi_{V_T}) + \left(\frac{I_b}{G_{m1}}\right)^2 \cdot \sigma_{\beta_1}^2 \cdot (1 + \xi_{\beta})$$
(2.46)

where  $\xi_{V_T}$  represents the  $V_T$ -mismatch contributions to the input-referred offset of the current mirrors relative to that of the differential pair

$$\xi_{V_T} = 2\left(\frac{G_{m2}}{G_{m1}}\right)^2 \cdot \frac{\sigma_{V_{T2}}^2}{\sigma_{V_{T1}}^2} + \left(\frac{G_{m3}}{A_1 G_{m1}}\right)^2 \cdot \frac{\sigma_{V_{T3}}^2}{\sigma_{V_{T1}}^2}$$
(2.47)

and  $\xi_{\beta}$  represents the  $\beta$ -mismatch contributions to the input-referred offset of the current mirrors relative to that of the differential pair

$$\xi_{\beta} = 2\frac{\sigma_{\beta_2}^2}{\sigma_{\beta_1}^2} + \frac{\sigma_{\beta_3}^2}{A_1^2 \sigma_{\beta_1}^2} \tag{2.48}$$

with

$$\sigma_{V_{T1}}^2 = \frac{A_{VTn}^2}{W_1 L_1},\tag{2.49}$$

$$\sigma_{V_{T2}}^2 = \frac{A_{VTp}^2}{W_2 L_2},\tag{2.50}$$

$$\sigma_{V_{T3}}^2 = \frac{A_{VTn}^2}{W_3 L_3},\tag{2.51}$$

and

$$\sigma_{\beta_1}^2 = \frac{A_{\beta n}^2}{W_1 L_1},\tag{2.52}$$

$$\sigma_{\beta_2}^2 = \frac{A_{\beta p}^2}{W_2 L_2},\tag{2.53}$$

$$\sigma_{\beta_3}^2 = \frac{A_{\beta n}^2}{W_3 L_3}. (2.54)$$

Replacing in (2.47) and (2.48) results in

$$\xi_{V_T} = 2\left(\frac{G_{m2}}{G_{m1}}\right)^2 \cdot \left(\frac{A_{VTp}}{A_{VTn}}\right)^2 \cdot \frac{W_1L_1}{W_2L_2} + \left(\frac{G_{m3}}{A_1 G_{m1}}\right)^2 \cdot \frac{W_1L_1}{W_3L_3}$$
(2.55)

and

$$\xi_{\beta} = 2\left(\frac{A_{\beta p}}{A_{\beta n}}\right)^{2} \cdot \frac{W_{1}L_{1}}{W_{2}L_{2}} + \frac{1}{A_{1}^{2}} \frac{W_{1}L_{1}}{W_{3}L_{3}}$$
(2.56)

Similarly to the flicker noise, the input-referred offset (variance or standard deviation) can be reduced by increasing the differential pair  $M_{1a}$ - $M_{1b}$  area  $W_1L_1$  but at the same time also increasing the area of the current mirrors  $W_2L_2$  (and hence  $W_{2c}L_{2c}$  and  $W_{2d}L_{2d}$ ) and depending on  $A_1$  also the area of the current mirror  $M_{3a}$ - $M_{3b}$   $W_{3a}L_{3a}$  and  $W_{3b}L_{3b}$ . This obviously comes at the cost of increased parasitic capacitances at nodes 2, 3 and 4 that will unavoidably reduce the phase margin.

Having done the small-signal, noise and offset analysis, we can now proceed with the design.

## Design

#### 3.1 Specifications

The OTA specifications are given in Table 3.1.



#### Warning

An important limitation of the IHP SC13G2 BiCMOS technology [5] is the high output conductance and hence limited intrinsic gain of nMOS transistors. Because of this, the specification on the DC gain, that was initially set to 80 dB, has been downgraded to 70 dB.

#### Note

The specifications given in Table 3.1 are simplified specifications. They are mainly targeting the achievement of a certain gain-bandwidth product GBW and DC gain at lowest current consumption. The GBW sets the differential pair transconductance while the DC gain sets the output conductance. There is an additional specification on the random input-referred offset voltage which, if not met, might eventually require to increase the transistors area. There are no specifications on thermal noise since the transconductance is set by the GBW. There are no specifications on the flicker noise but if the corner frequency was set lower this would required to increase the transistors area. There are also no specifications on the slew-rate, which might be small because of the low-power objective. Finally, there are many more specifications such as CMRR, PSRR, input common-mode voltage range, output-voltage swing, etc... that are not discussed in this example.

Table 3.1: OTA specifications.

Specification	Symbol	Value	Unit
Minimum DC gain	$A_{dc}$	70	dB
Minimum gain-bandwidth product	GBW	1	MHz
Load capacitance	$C_L$	1	pF
Maximum input-referred random offset voltage	$V_{os}$	10	mV
Phase margin	PM	60	0

#### 3.2 Process

We will design the cascode gain stage for the open source IHP 13G2 BiCMOS process [5]. The physical parameters are given in Table 3.2, the global process parameters in Table 3.3 and finally the MOSFET parameters in Table 3.4.

## ⚠ Warning

The matching parameters for IHP  $130\mathrm{nm}$  are unknown. We will use those from a generic  $180\mathrm{nm}$  technology.

Table 3.2: Physical parameters

Parameter	Value	Unit
$\overline{T}$	300	K
$U_T$	25.865	mV

Table 3.3: Process parameters.

Parameter	Value	Unit	Comment
$t_{ox}$	2.24	nm	SiO <sub>2</sub> oxyde thickness
$C_{ox}$	15.413	$\frac{fF}{\mu m^2}$	Oxyde capacitance per unit area
$V_{DD}$	1.2	$\overline{V}$	Nominal supply voltage
$L_{min}$	130	nm	Minimum drawn gate length
$W_{min}$	150	nm	Minimum drawn gate width
$z_1$	340	nm	Minimum outer diffusion width
$z_2$	389	nm	Minimum diffusion width between two fingers

Table 3.4: Transistors parameters.

Parameter	nMOS	pMOS	Unit
Length and width correction parameters for current			
DL	59	51	nm
DW	-20	30	nm
length and width correction for intrinsic and overlap capacitances			
DLCV	93	146	nm
DWCV	-10	15	nm
Length and width correction parameter for fringing capacitances			
DLGCV	34	96	nm
DWGCV	10	-15	nm
Long-channel sEKV parameters parameters			
n	1.22	1.23	-
$I_{spec}\Box$	708	245	nA
$V_{T0}$	246	365	mV
Short-channel sEKV parameters parameters		24.0	
$L_{sat}$	7.1	24.9	nm $V$
$\lambda$	1.375	6.078	$\frac{V}{\mu m}$
Junction capacitances parameters			f E
$C_J$	0.976	0.863	$\frac{JF}{\mu m^2}$
$C_{JSWSTI}$	0.025	0.032	$\frac{fF}{\mu m}$
$C_{JSWGAT}$	0.03	0.027	$\frac{\frac{fF}{\mu m^2}}{\frac{fF}{\mu m}}$ $\frac{fF}{\mu m}$
Overlap capacitances parameters			μπι
$C_{GSo}$	0.453	0.443	$\frac{fF}{um}$
$C_{GDo}$	0.453	0.443	$\frac{\frac{fF}{\mu m}}{\frac{fF}{\mu m}}$
$C_{GBo}$	0	0.022	$rac{\mu m}{fF}$
$\sim$ $GB_0$	O	0.022	$\mu m$

Table 3.4: Transistors parameters.

Parameter	nMOS	pMOS	Unit
Fringing capacitances parameters			
$C_{GSf}$	0.2	0.1	$rac{fF}{\mu m} rac{fF}{fF}$
$C_{GDf}$	0.2	0.1	$\frac{\widetilde{fF}}{\mu m}$
Flicker noise parameters			<i>p</i>
$K_F$	2.208e-24	1.2e-23	VAs
AF	1	1	-
ho	0.008642	0.04697	$\frac{Vm^2}{As}$
Matching parameters			
$A_{VT}$	5	5	$mV \cdot \mu m$
$A_eta$	1	1	$\% \cdot \mu m$

#### 3.3 Design procedure

#### ! Important

For this process, the transistor dimensions are rounded to 10nm. We also will ignore the length and width reduction parameters DL and DW. The main reason is that most of the transistor length and width are sufficiently large that ignoring these parameters has little impact.

We need to start with choosing the current gain  $A_3$ . We have seen that having a current gain  $A_3 > 1$  improves the transconductance but at the cost of a higher thermal noise excess factor  $\gamma_{ota}$ . We therefore will set to

 $A_1 = 1$ ,

 $A_2 = 1$ ,

 $A_3 = 1.$ 

Since  $A_1 = A_2 = A_3 = 1$ , transistors  $M_{2a}$ ,  $M_{2b}$ ,  $M_{2c}$  and  $M_{2d}$  are all identical and so are  $M_{3a}$  and  $M_{3b}$ . We therefore have the following variables:

- $M_{1a}$ - $M_{1b}$ :  $W_1$ ,  $L_1$  and  $I_b$ . Note that the current  $I_b$  is set by  $G_{m1}$  because  $M_{1a}$ - $M_{1b}$  are biased in weak inversion,
- $M_{2a}$ - $M_{2c}$  and  $M_{2b}$ - $M_{2d}$ :  $IC_2$ ,  $W_2$  and  $L_2$  since the current is already set,
- $M_{3a}$ - $M_{3b}$ :  $IC_3$ ,  $W_3$  and  $L_3$  since the current is already set,
- $M_4$ :  $IC_4$ ,  $W_4$  and  $L_4$  since the current is already set,
- $M_7$ :  $IC_7$ ,  $W_7$  and  $L_7$  since the current is already set,
- $M_{5a}$ - $M_{5b}$ :  $IC_5$ ,  $W_5$  and  $L_5$  since the current is already set.

We start sizing the differential pair  $M_{1a}$ - $M_{1b}$ .

#### 3.3.1 Sizing the differential pair $M_{1a}$ - $M_{1b}$

In this example there is no specification on the input-referred white noise. Therefore the transconductance  $G_{m1}$  is set by the gain-bandwidth product according to

$$GBW = \frac{G_{m1}}{2\pi C_{out}},\tag{3.1}$$

where  $G_{m1}$  is the gate transconductance of  $M_{1a}$  and  $M_{1b}$  and  $C_{out}$  the total output capacitance

$$C_{out} = C_o + C_L \tag{3.2}$$

with  $C_o$  the parasitic capacitance at the output node and  $C_L$  the specified load capacitance.

In order to minimize the input-referred noise and offset, the input differential pair should be biased in weak inversion. The transconductance  $G_{m1}$  in deep weak inversion is then given by

$$G_{m1} = \frac{I_b}{nU_T}. (3.3)$$

The bias current  $I_b$  is the current flowing in each transistor  $M_{1a}$  and  $M_{1b}$  when the input differential voltage is zero. The bias current provided by  $M_{5b}$  is therefore  $2I_b$ . The bias current must satisfy the following inequality:

$$I_b \ge 2\pi n_{0n} U_T C_{out} GBW_{min}. \tag{3.4}$$

which for the given specifications gives  $I_{b,min} = 198 \ nA$ . The corresponding slew-rate is then equal to  $SR_{min} = 198 \ mV/\mu s$  which we will consider as sufficient.

#### Important

If the slew-rate is not sufficient, the bias current  $I_b$  should be increased resulting in a higher current and power consumption. Other options include the use of a class AB OTA [8] or a dynamic/adaptive biasing OTA [9].

As we will see below, the cascode transistors  $M_4$  and  $M_7$  will be biased in weak inversion to save voltage headroom at the output and preserve the output voltage swing of the symmetrical OTA. They will therefore be rather large transistors. Since they are connected to the output, they will increase the parasitic capacitance at the output  $C_o$  due mostly to the junction capacitances. To have sufficient margin, we set  $I_b = 280 \ nA$  and the inversion coefficient to  $IC_1 = 0.1$ . The transconductance can be calculated from the  $G_m/I_D$  function as  $G_{m1} = 8.129 \ \mu A/V$ . This leads to a gain-bandwidth product

$$GBW = \frac{G_{m1}}{2\pi C_L} = 1.3 MHz,$$

which is slightly higher than the target specification offering some margin. Knowing the drain current  $I_{D1}$  and the inversion coefficient, we can calculate the W/L aspect ratio for  $M_{1a}$ - $M_{1b}$  as  $W_1/L_1 = 4.0$ .

Before finalizing the sizing of the differential pair, we first will size the current mirrors.

#### 3.3.2 Sizing the pMOS current mirrors $M_{2a}$ - $M_{2c}$ and $M_{2b}$ - $M_{2d}$

The gate voltage of  $M_{2a}$ - $M_{2b}$  should be set as low as possible for a given maximum common mode input voltage  $V_{ic,max}$  still keeping  $M_{1a}$ - $M_{1b}$  in saturation. The source-to-gate voltage of  $M_{2a}$ - $M_{2b}$   $V_{SG2}$  is given by

$$V_{SG2} = V_{DD} - V_{icmax} + V_{GS1} - V_{DSsat1}. (3.5)$$

The gate-to-source voltage  $V_{GS1}$  and the saturation voltage  $V_{DSsat1}$  of  $M_{1a}$ - $M_{1b}$  are given by  $V_{GS1} = 176 \ mV$  and  $V_{DSsat1} = 105 \ mV$ . For a maximum input common-mode voltage  $V_{ic,max} = 0.7 \ V$ , the minimum source-to-gate voltage is given by  $V_{SG2} = 572 \ mV$ , corresponding to an inversion coefficient  $IC_2 = 10.265$ .

We can set  $V_{SG2}$  to  $V_{SG2} = V_{DD}/2 = 600~mV$  which corresponds to an inversion coefficient  $IC_2 = 12.882$  and a saturation voltage  $V_{DSsat2} = 213~mV$ . The specific current  $I_{spec}$ , transconductance  $G_m$  and W/L are then given by  $I_{spec2} = 21.74~nA$ ,  $G_{m2} = 2.134~\mu A/V$  and  $W_2/L_2 = 0.089$ .

We now have to make sure that the non-dominant poles  $f_{p2}$  and  $f_{p4}$  at nodes 2 and 4 are sufficiently higher than the GBW to insure the desired phase margin. The non-dominant pole is given by

$$\omega_{p2} = \frac{G_{m2}}{C_2},\tag{3.6}$$

where  $C_2$  is the total capacitance at node 2

$$C_2 = 2(C_{GS2} + C_{GB2}). (3.7)$$

Assuming  $M_{2a}$ - $M_{2b}$  are in saturation, the gate-to-source capacitance  $C_{GS2}$  is given by

$$C_{GS2} \cong W_2 L_2 C_{ox} \cdot c_{qsi} + (C_{GSop} + C_{GSfp}) \cdot W_2,$$
 (3.8)

where  $c_{gsi}$  is the intrinsic gate-to-source capacitance normalized to the total gate area  $WLC_{ox}$ , which is typically equal to 2/3 in strong inversion and is proportional to IC in weak inversion.

The gate-to-bulk capacitance  $C_{GB2}$  is given by

$$C_{GB2} \cong W_2 L_2 C_{ox} \cdot c_{abi} + C_{GBop} \cdot W_2, \tag{3.9}$$

where  $c_{gbi}$  is the gate-to-bulk intrinsic capacitance normalized to the total gate area  $W L C_{ox}$  and given by

$$c_{gbi} = \frac{n-1}{n} \cdot c_{gsi}. (3.10)$$

The capacitance at node 2 then scales with  $W_2$  and  $L_2$  according to

$$C_2 = W_2 L_2 \cdot C_{WL} + W_2 \cdot C_W, \tag{3.11}$$

with

$$C_{WL} = 2C_{ox} \cdot (c_{qsi} + c_{qbi}), \tag{3.12}$$

$$C_W = 2(C_{GSop} + C_{GSfp} + G_{GBop}). (3.13)$$

We already have set the inversion coefficient  $IC_2 = 12.882$ , from which we can calculate  $c_{gsi} = 0.566$  and  $c_{gbi} = 0.081$ . Since the W/L has already been set by the transconductance and the current, we can derive  $W_2$  and  $L_2$  for achieving a given capacitance  $C_2$  according to

$$W_2 = \frac{-C_W \cdot W_2 / L_2 + \sqrt{W_2 / L_2} \cdot \sqrt{4 C_2 C_{WL} + C_W^2 \cdot W_2 / L_2}}{2 C_{WL}},$$
(3.14)

$$L_2 = \frac{W_2}{W_2/L_2}. (3.15)$$

Setting the non-dominant pole  $f_{p2}$  to 10 times the GBW, we get  $C_2 = 26$  fF,  $L_2 = 3.83 \ \mu m$  and  $W_2 = 340 \ nm$ .

Since  $A_1 = A_3 = 1$ ,  $M_{2a}$ ,  $M_{2b}$ ,  $M_{2c}$  and  $M_{2d}$  are all identical and hence  $W_{2a} = W_{2b} = W_{2c} = W_{2d} = 340 \ nm$  and  $L_{2a} = L_{2b} = L_{2c} = L_{2d} = 3.83 \ \mu m$ .

We next size the nMOS current mirror  $M_{3a}$  and  $M_{3b}$ .

#### 3.3.3 Sizing the nMOS current mirror M<sub>3a</sub> and M<sub>3b</sub>

To size  $M_{3a}$  and  $M_{3b}$  we need to

- consider the output swing and
- make sure that  $M_{2c}$  remains in saturation for the chosen overdrive voltage chosen for  $M_{3a}$ .

Let's start maximizing the output swing assuming that we bias the cascode transistor  $M_7$  in weak inversion for minimum saturation voltage and maximum  $G_m/I_D$ . We set the inversion coefficient of  $M_7$  to  $IC_7 = 0.1$ . The saturation voltage of  $M_7$  is then given by  $V_{DSsat7} = 105 \ mV$ .

Let's say that we want an output swing of 400 mV. This means that we have 800 mV to share between the positive and negative saturation voltages which we decide to split equally. This means 400 mV for the saturation voltages of  $M_7$  and  $M_{3b}$  which leaves a saturation voltage for  $M_{3b}$  of  $V_{DSsat3} = 295 \ mV$ . This corresponds to an inversion coefficient  $IC_3 = 28.6$ .

We now can check whether with the chosen inversion coefficient for  $M_{3b}$ ,  $M_{2c}$  remains in saturation. The gate-to-source voltage of  $M_{3a}$  is  $V_{GS3a}=603~mV$ , giving a source to-drain voltage for  $M_{2c}$   $V_{SD2c}=597~mV$ , which is larger than its saturation voltage  $V_{DSsat2c}=213~mV$ .

Knowing the current and the  $IC_2 = 28.6$ , we can deduce  $I_{spec3} = 9.798 \ nA$ ,  $W_3/L_3 = 1.4\text{e-}02$  and  $G_{m3} = 1.500 \ \mu A/V$ .

Similarly to what was done for transistor  $M_{2a}$ - $M_{2c}$ , we need to make sure that the non-dominant pole  $f_{p3}$  at node 3 remains much higher than the GBW. Setting  $f_{p3}/GBW = 10$  and proceeding in a similar way we get  $f_{p3}/GBW = 10$  with  $C_3 = 18.4$  fF resulting in  $W_3 = 110$  nm and  $L_3 = 7.95$   $\mu$ m.

We see that  $W_3$  is smaller than the minimum width. If we don't want to increase  $W_3 L_3$  and hence  $C_3$ , we need to reduce the inversion coefficient  $IC_3$ . We can find the IC such that  $W_3 = W_{min}$  for the given  $f_{p3}$  by looking at Figure 3.1.

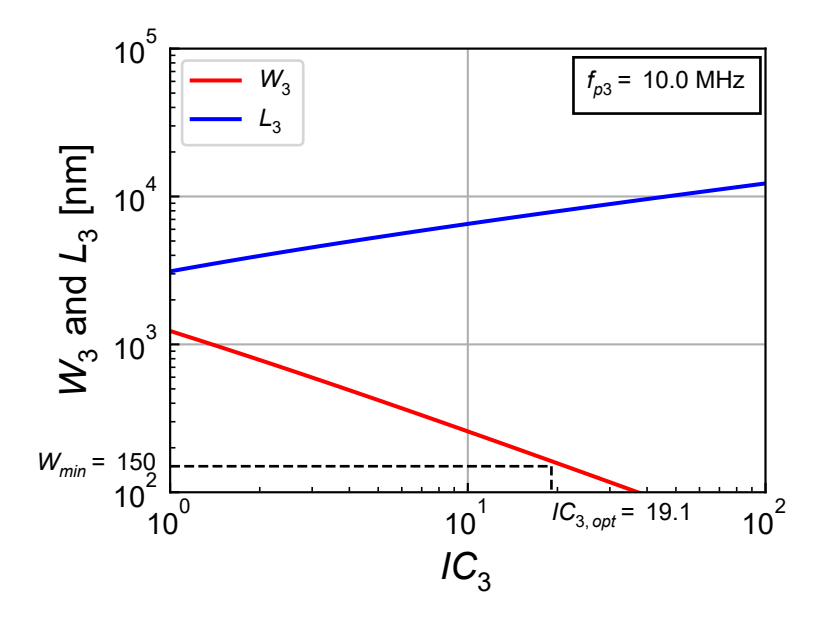


Figure 3.1: Length  $L_3$  and width  $W_3$  of  $M_3$  versus  $IC_3$  for a given  $f_{p3}/GBW$  ratio.

We get  $IC_3 = 19.1$ ,  $W_3 = 150 \ nm$  and  $L_3 = 7.24 \ \mu m$  with  $C_3 = 13.3 \ fF$  and  $f_{p3}/GBW = 10$ .

The inversion coefficient of  $M_{3a}$ - $M_{3b}$  is therefore reduced from 28.6 to 19.1 in order to maintain a reasonable parasitic capacitance at node 3 to make sure that  $f_{p3}$  is 10-times higher than the GBW.

 $M_{3b}$  is identical to  $M_{3a}$  and therefore  $W_{3a} = W_{3b} = 150 \ nm$  and  $L_{3a} = L_{3b} = 7.24 \ \mu m$ .

#### 3.3.4 Sizing the cascode transistors M<sub>4</sub>-M<sub>7</sub>

The cascode transistors are sized according to the desired DC gain given by

$$A_{dc} = \frac{A_3 \cdot G_{m1}}{G_o} \tag{3.16}$$

with

$$G_o = \frac{G_{ds3b} \cdot G_{ds7}}{G_{ms7}} + \frac{G_{ds2d} \cdot G_{ds4}}{G_{ms4}}$$
(3.17)

The minimum DC gain specification is given by  $A_{dc} = 3.2 \text{e} + 03$  or  $A_{dc} = 70$  dB. Since the transconductance  $G_{m1}$  is already set by the GBW, the output conductance at the output node  $G_o$  is then given by  $G_o = G_{m1}/A_{dc} = 2.571 \ nA/V$ . We will split the output conductance equally between the nMOS and pMOS cascodes. We already have set the inversion coefficient of  $M_7$  to  $IC_7 = 0.1$ . Knowing the current, we can deduce the specific current  $I_{spec7} = 2.8 \ \mu A$  and the aspect ratio  $W_7/L_7 = 4.0$ . Knowing the current and  $IC_7$  we can get  $G_{ms7} = 9.917 \ \mu A/V$ .

We already have chosen the length of  $M_{3a}$ - $M_{3b}$   $L_3 = 7.24 \ \mu m$ . The output conductance of  $M_{3b}$  can then be estimated to  $G_{ds3} = 28.113 \ nA/V$ . We can then deduce the output conductance of  $M_7$  as  $G_{ds7} = 453.389 \ nA/V$  from which we deduce its length  $L_7 = 0.45 \ \mu m$ .

To have some margin because of the high output conductance of nMOS transistors in this technology, we choose a slightly longer length  $L_7 = 1.00 \ \mu m$ . Keeping the same  $W_7/L_7 = 4.0$ , we get  $W_7 = 3.95 \ \mu m$ .

The minimum value of the bias voltage  $V_{b2}$  is set such that  $M_{3b}$  remains in saturation

$$V_{b2,min} = V_{DSsat3} + V_{GS2}. (3.18)$$

The saturation voltage of  $M_{3b}$  is equal to  $V_{DSsat3} = 249 \ mV$  and the  $V_{GS}$  voltage of  $M_7$  is  $V_{GS7} \cong 246 \ mV$ , which results  $V_{b2,min} = 495 \ mV$ . For convenience we choose  $V_{b2} = V_{DD}/2 = 600 \ mV$ .

For  $M_4$  we set the same inversion coefficient as  $M_7$   $IC_4 = IC_7 = 0.1$ , from which we get its saturation voltage  $V_{DSsat4} = 105$  mV. Knowing the current and the IC we can deduce  $I_{spec4} = 2.8$   $\mu A$  and  $W_4/L_4 = 11.4$ . The source transconductance of  $M_4$  is then given by  $G_{ms4} = 9.917$   $\mu A/V$ . The output conductance of  $M_{2d}$  can be estimated as  $G_{ds2} = 12.028$  nA/V. We can then deduce the output conductance of  $M_4$   $G_{ds4} = 1059.674$  nA/V, from which we can calculate the length  $L_4 = 40$  nm, which is smaller than the minimum length.

We could choose  $L_4 = L_{min}$ , but in order to have some margin on the DC gain, we choose  $L_4 = 250$  nm. Keeping the same  $W_4/L_4 = 11.4$ , this leads to  $W_4 = 2.86 \ \mu m$ .

The maximum value of the bias voltage  $V_{b1}$  is limited by the saturation voltage of  $M_{2d}$  according to

$$V_{b1,max} = V_{DD} - V_{SDsat2d} - V_{SG4}. (3.19)$$

The saturation voltage of  $M_{2d}$  is  $V_{SDsat2}=213~mV$  and the source-to-gate voltage of  $M_4$  is  $V_{SG4}\cong 365~mV$ , leading to  $V_{b1,max}\cong 622.453~mV$ . For convenience, we can also set  $V_{b1}=V_{DD}/2=500~mV$ .

We can now check the resulting DC gain. The output conductance of the nMOS and pMOS cascodes are  $G_{on} = 577.300 \ pA/V$  and  $G_{op} = 223.510 \ pA/V$ , respectively. This results in a total output conductance  $G_{o} = 800.810 \ pA/V$  and a DC gain  $A_{dc} = 1e+04$  or  $A_{dc} = 80.1$  dB, which is 10 dB higher than the specifications.

#### 3.3.5 Sizing the nMOS current mirror M<sub>5a</sub>-M<sub>5b</sub>

Finally we need to size  $M_{5a}$ - $M_{5b}$ . The minimum input common mode voltage  $V_{ic,min}$  is limited by the saturation voltage of  $M_{5b}$  according to

$$V_{ic,min} = V_{GS1} + V_{DSsat5b}. (3.20)$$

Since  $M_{1a}$ - $M_{1b}$  are in a separate well, their gate-to-source voltage is  $V_{GS1} = V_{T0n} + n U_T (v_p - v_s) \cong 176$  mV. Setting the minimum input common mode voltage to  $V_{ic,min} = 400 \ mV$  leads to the maximum saturation voltage of  $M_{5b} \ V_{DSsat5} = V_{ic,min} - V_{GS1} \cong 224 \ mV$ . The corresponding inversion coefficient of  $M_{5b}$  is  $IC_5 = 14.7$ . From  $I_b$  and  $IC_5$  we get  $I_{spec5} = 38.119 \ nA$  and  $W_5/L_5 = 5.382$ e-02. With such a low W/L ratio, we need to set  $W_5$  to the minimum width  $W_5 = W_{min} = 150 \ nm$  from which we deduce  $L_5 = 2.79 \ \mu m$ .

Transistor  $M_{5a}$  is identical to  $M_{5b}$  and hence  $W_{5a} = W_{5b} = 150 \ nm$  and  $L_{5a} = L_{5b} = 2.79 \ \mu m$ .

The sizing process is almost finished, but we still need to finalize the sizing of the differential pair  $M_{1a}$ - $M_{1b}$ .

#### 3.3.6 Final sizing of the differential pair $M_{1a}$ - $M_{1b}$

We haven't finalized the sizing of  $M_{1a}$ - $M_{1b}$ . We already have the W/L ratio but still need to set  $W_1$  and  $L_1$ . We don't have any specifications on the noise and particularly the corner frequency, while the white noise is already set by the transconductance  $G_{m_1}$ .

Since the current mirrors current gains are all unity  $A_1 = A_2 = A_3 = 1$ , the transistors  $M_{2a}$ ,  $M_{2b}$ ,  $M_{2c}$  and  $M_{2d}$  are all identical. In this case the contributions of the current mirrors to the input-referred flicker noise relative to the contribution of the differential pair is captured by the  $\eta_{fl}$  parameter recalled below

$$\eta_{fl} = 2 \frac{\rho_p}{\rho_n} \cdot \left(\frac{G_{m2}}{G_{m1}}\right)^2 \frac{W_1 L_1}{W_2 L_2} + \left(\frac{G_{m3}}{G_{m1}}\right)^2 \cdot \frac{W_1 L_1}{W_3 L_3}.$$
 (3.21)

The ratio of the flicker noise parameter of pMOS transistors to that of nMOS transistors is given by  $\rho_p/\rho_n = 5.435$ , which is rather large. The square of the transconductance ratio  $(G_{m1}/G_{m2})^2 = 14.506$  should compensate for this large  $\rho_p/\rho_n$  ratio. We can try to make the contribution of the input differential pair equal to the contribution of the current mirrors (i.e. set  $\eta_{fl} = 1$ ). This results in  $W_1 \cdot L_1 = 1.610 \ \mu m^2$ .

Since we already have  $W_1/L_1$  we can deduce  $W_1=2.52~\mu m$  and  $L_1=640~nm$ . Since transistor  $M_{1a}$  is identical to  $M_{1b}$ , we have  $W_{1a}=W_{1b}=2.52~\mu m$  and  $L_{1a}=L_{1b}=640~nm$ .

The relative contribution to the input-referred flicker noise of the pMOS current mirrors  $M_{2a}$  to  $M_{2d}$  is 0.928, whereas that of the nMOS current mirror  $M_{3a}$  and  $M_{3b}$  is 0.074. This leads to  $\eta_{fl} = 1.002$ , which is close to the desired  $\eta_{fl} \cong 1$ .

We now have finalized the design. We can still check the thermal noise. The OTA thermal noise excess factor  $\gamma_{ota}$  and the input-referred white noise PSD are given by

$$\eta_{th} = 0.919,$$

$$\gamma_{ota} = 2.4,$$

$$R_{ninth} = 296.1 \ k\Omega,$$

$$S_{ninth} = 4.9e-15 \ \frac{V^2}{Hz},$$

$$\sqrt{S_{ninth}} = 70.1 \ \frac{nV}{\sqrt{Hz}},$$

$$10 \cdot \log(S_{ninth}) = -143.1 \ \frac{dBv}{\sqrt{Hz}}.$$

This sets the corner frequency to  $f_k = 72.4 \ kHz$ .

The design is now finalized and is summarized in the section.

## 3.4 Summary

#### 3.4.1 Specifications

The specifications are recalled in Table 3.5.

Table 3.5: OTA specifications.

Specification	Symbol	Value	Unit
Minimum DC gain	$A_{dc}$	70	dB
Minimum gain-bandwidth product	GBW	1	MHz
Load capacitance	$C_L$	1	pF
Maximum input-referred random offset voltage	$V_{os}$	10	mV
Phase margin	PM	60	0

#### 3.4.2 Bias

The bias information are summarized in Table 3.6.

Table 3.6: OTA bias.

Bias voltage or current	Symbol	Value	Unit
Supply voltage	$V_{DD}$	1.2	V
Bias current	$I_b$	280.0	nA
Cascode bias voltage	$V_{b1}$	0.5	V
Cascode bias voltage	$V_{b2}$	0.6	V

#### 3.4.3 Transistor information

The transistor sizes and large-signal variables are summarized in Table 3.7, whereas Table 3.8 gives the small-signal and thermal noise parameters. An Excel table is generated with more information (e.g. all the parasitic capacitances).

Table 3.7: Transistor size and bias information.

Transistor	$W [\mu m]$	$L [\mu m]$	$I_D [nA]$	$I_{spec} [nA]$	IC	$V_G - V_{T0} [mV]$	$V_{DSsat} [mV]$
M1a	2.52	0.64	280	2789	0.1	-47	105
M1b	2.52	0.64	280	2789	0.1	-47	105
M2a	0.34	3.83	280	22	12.9	155	213
M2b	0.34	3.83	280	22	12.9	155	213
M2c	0.34	3.83	280	22	12.9	155	213
M2d	0.34	3.83	280	22	12.9	155	213
M3a	0.15	7.24	280	15	19.1	194	249
M3b	0.15	7.24	280	15	19.1	194	249
M4	2.86	0.25	280	2798	0.1	-46	105
M5a	0.15	2.79	560	38	14.7	169	224

Table 3.7: Transistor size and bias information.

Transistor	$W [\mu m]$	$L [\mu m]$	$I_D [nA]$	$I_{spec} [nA]$	IC	$V_G - V_{T0} [mV]$	$V_{DSsat} [mV]$
M5b	0.15	2.79	560	38	14.7	169	224
M7	3.95	1.00	280	2798	0.1	-47	105

Table 3.8: Transistor small-signal and thermal noise parameters.

Transistor	$G_{spec} \left[ \mu A/V \right]$	$G_{ms} \left[ \mu A/V \right]$	$G_m \left[ \mu A/V \right]$	$G_{ds} [nA/V]$	$\gamma_n$
M1a	107.827	9.914	8.126	318.182	0.627
M1b	107.827	9.914	8.126	318.182	0.627
M2a	0.840	2.624	2.133	12.028	0.770
M2b	0.840	2.624	2.133	12.028	0.770
M2c	0.840	2.624	2.133	12.028	0.770
M2d	0.840	2.624	2.133	12.028	0.770
M3a	0.567	2.210	1.812	28.113	0.772
M3b	0.567	2.210	1.812	28.113	0.772
M4	108.186	9.917	8.062	184.271	0.632
M5a	1.472	4.958	4.064	145.976	0.767
M5b	1.472	4.958	4.064	145.976	0.767
M7	108.169	9.916	8.128	203.636	0.627

## **4 OTA Characteristics**

In this section, we check whether the specs are achieved.

#### 4.1 Open-loop gain

We can calculate the various OTA features related to the open-loop transfer function, which are given in Table 4.1.

Symbol	Theoretical Value	Unit
$\overline{A_{dc}}$	80	$\overline{dB}$
$G_{m1}$	8.126	$\mu A/V$
$G_{m2}$	2.133	$\mu A/V$
$G_{m3}$	1.812	$\mu A/V$
$f_0$	126.603	Hz
GBW	1.285	MHz
$f_{p2}$	12.875	MHz
$f_{p3}$	12.937	MHz
$f_{p4}$	12.875	MHz

Table 4.1: OTA gain variables.

The gain-bandwidth product from the specifications is repeated here

GBW = 1.000 MHz (from spec).

The estimated value assuming that all the non-dominant poles are much higher than the GBW is given by

 $GBW_{est} = 1.285 \text{ MHz}$  (estimation).

The GBW accounting for the effect of the additional non-dominant poles is given by

 $GBW_{the} = 1.274 \text{ MHz (theory)}.$ 

We see that there is only a small difference between  $GBW_{est}$  and  $GBW_{the}$ , which confirms that the non-dominant poles are sufficiently far from GBW as stated in Table 4.1.

We can now plot the gain response using the variables given in Table 4.1. It is shown in Figure 4.1.

### 4.2 Input-referred noise

We can now compute all the parameters needed for the calculation of the OTA thermal noise excess factor and its input-referred thermal noise PSD and resistance. They are given in Table 4.2.

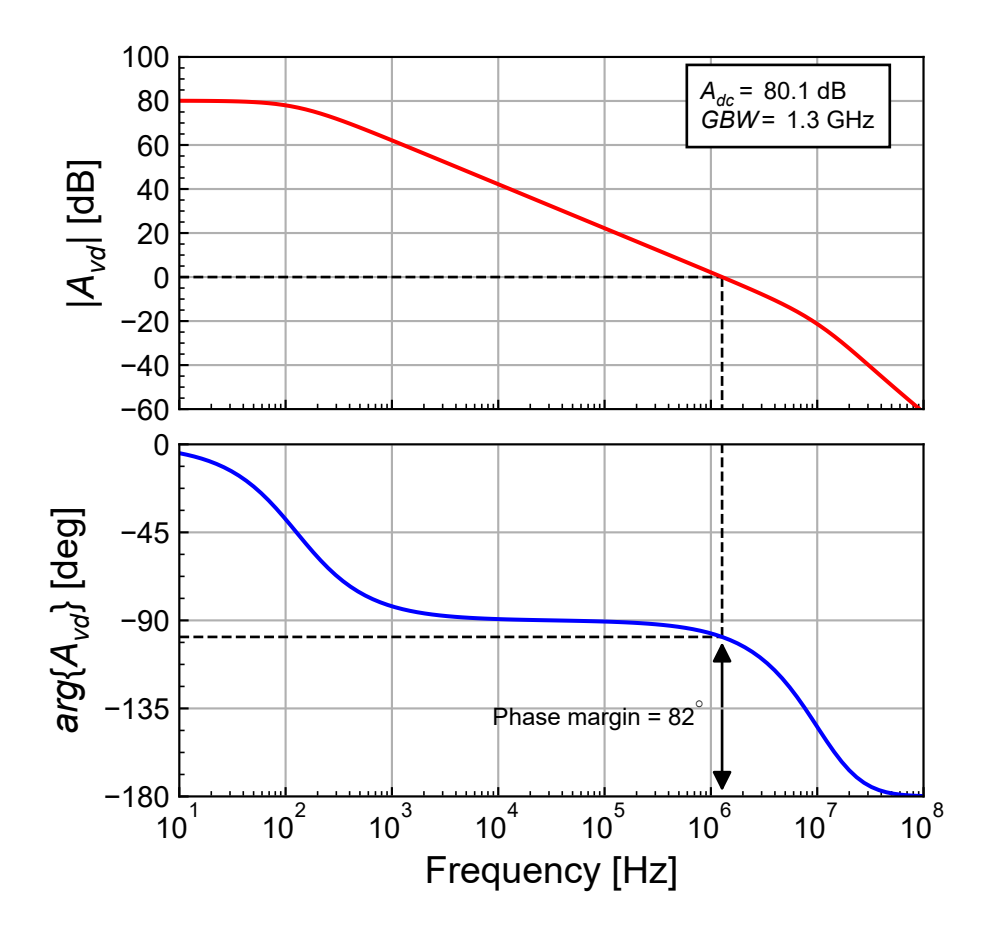


Figure 4.1: OTA theoretical transfer function.

Table 4.2: OTA thermal noise parameters.

-		
Symbol	Theoretical Value	$\operatorname{Unit}$
$\overline{G_{m1}}$	8.126	$\mu A/V$
$G_{m2}$	2.133	$\mu A/V$
$G_{m3}$	1.812	$\mu A/V$
$G_{m1}/G_{m2}$	3.809	_
$G_{m1}/G_{m3}$	4.485	-
$\gamma_{n1}$	0.627	-
$\gamma_{n2}$	0.77	-
$\gamma_{n3}$	0.772	-
$\eta_{th}$	0.919	-
$\gamma_{ota}$	2.407	-
$R_{nt}$	296.239	$k\Omega$
$S_{ninth}$	4.9e-15	$V^2/Hz$
$\sqrt{S_{ninth}}$	70.075	$nV/\sqrt{Hz}$
$10 \cdot \log(S_{ninth})$	-143.089	$dBv/\sqrt{Hz}$

From the value of  $\eta_{th} = 0.919$  in Table 4.2, we see that the current mirrors  $M_{2a}$ - $M_{2b}$ - $M_{2c}$ - $M_{2d}$  and  $M_{3a}$ - $M_{3b}$  contribute about equally to the OTA input-referred thermal noise PSD. The OTA thermal noise excess factor is therefore about twice that of the differential pair  $2 \gamma_{n1}$ .

We can now compute all the parameters needed for the calculation of the input-referred flicker noise and the corner frequency. They are given in Table 4.3.

Table 4.3: OTA flicker noise parameters.

Symbol	Theoretical Value	Unit
$-\frac{(G_{m1}/G_{m2})^2}{}$	14.5	-
$(G_{m1}/G_{m3})^2$	20.1	-
$ ho_p/ ho_n$	5.4	-
$rac{W_1 \cdot L_1}{W_2 \cdot L_2}$	1.2	-
$\frac{W_1 \cdot L_1}{W_3 \cdot L_3}$	1.8	-
$\eta_{fl}$	1.003	-
$\sqrt{S_{ninfl}(1Hz)}$	18.1	$\mu V/\sqrt{Hz}$
$10 \cdot \log(S_{ninfl}(1 Hz))$	-94.8	$dBv/\sqrt{Hz}$
$f_k$	66.9	kHz

Similarly to thermal noise, from the value of  $\eta_{fl} = 1.003$  in Table 4.3, we see that the current mirrors  $M_{2a}$ - $M_{2b}$ - $M_{2c}$ - $M_{2d}$  and  $M_{3a}$ - $M_{3b}$  contribute about equally to the OTA input-referred flicker noise PSD, despite the large  $\rho_p/\rho_n = 5.435$  ratio and the smaller area of the current mirrors compared to the differential pair. This is achieved because of the high gains  $(G_{m1}/G_{m2})^2 = 14.5$  and  $(G_{m1}/G_{m3})^2 = 20.1$ .

We can plot the input-referred noise PSD which is shown in Figure 4.2. The corner frequency is estimated at  $f_k = 66.9 \ kHz$ .

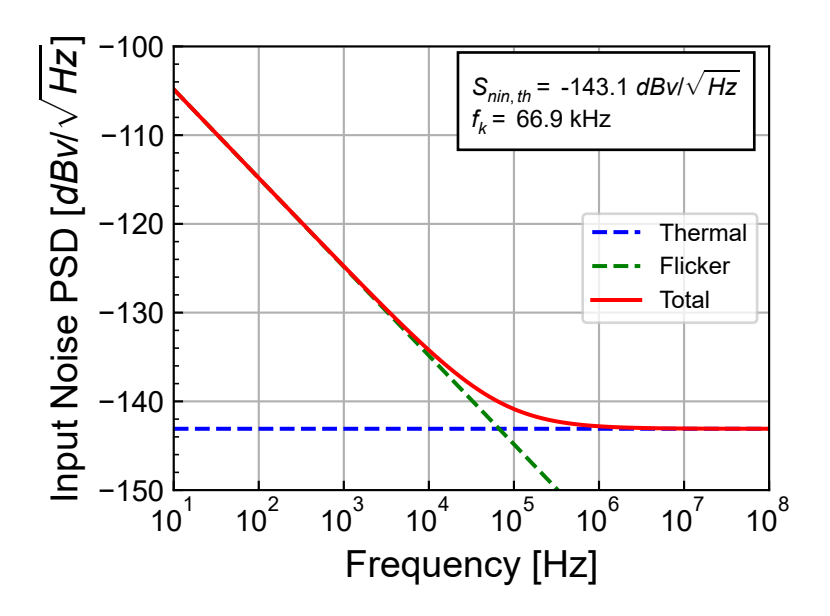


Figure 4.2: OTA theoretical input-referred noise PSD.

## 4.3 Input-referred offset voltage

The variance of the input-referred offset for  $A_1 = A_2 = A_3 = 1$  is given by (2.46) which can be rewritten as

$$\sigma_{V_{os}}^2 = \sigma_{V_T}^2 + \sigma_{\beta}^2 \tag{4.1}$$

where

$$\sigma_{V_T}^2 = \sigma_{V_{T_1}}^2 \cdot (1 + \xi_{V_T}) \tag{4.2}$$

and

$$\sigma_{\beta}^2 = \left(\frac{I_b}{G_{m1}}\right)^2 \cdot \sigma_{\beta_1}^2 \cdot (1 + \xi_{\beta}). \tag{4.3}$$

 $\xi_{V_T}$  represents the  $V_T$ -mismatch contributions to the input-referred offset of the current mirrors relative to that of the differential pair. It is given by (2.55) which is repeated here

$$\xi_{V_T} = 2\left(\frac{G_{m2}}{A_1 G_{m1}}\right)^2 \cdot \left(\frac{A_{VTp}}{A_{VTn}}\right)^2 \cdot \frac{W_1 L_1}{W_2 L_2} + \left(\frac{G_{m3}}{G_{m1}}\right)^2 \cdot \frac{W_1 L_1}{W_3 L_3} \tag{4.4}$$

and  $\xi_{\beta}$  represents the  $\beta$ -mismatch contributions to the input-referred offset of the current mirrors relative to that of the differential pair. It is given by (2.56) which is repeated below

$$\xi_{\beta} = 2\left(\frac{A_{\beta p}}{A_{\beta n}}\right)^{2} \cdot \frac{W_{1}L_{1}}{W_{2}L_{2}} + \frac{1}{A_{1}^{2}} \cdot \frac{W_{1}L_{1}}{W_{3}L_{3}}.$$
(4.5)

with

$$\sigma_{VT1}^2 = \frac{A_{VTn}^2}{W_1 L_1},\tag{4.6}$$

$$\sigma_{V_{T2}}^2 = \frac{A_{VTp}^2}{W_2 L_2},\tag{4.7}$$

$$\sigma_{V_{T3}}^2 = \frac{A_{VTn}^2}{W_3 L_3},\tag{4.8}$$

and

$$\sigma_{\beta 1}^2 = \frac{A_{\beta n}^2}{W_1 L_1},\tag{4.9}$$

$$\sigma_{\beta 2}^2 = \frac{A_{\beta p}^2}{W_2 L_2},\tag{4.10}$$

$$\sigma_{\beta 3}^2 = \frac{A_{\beta n}^2}{W_3 L_3}. (4.11)$$

The parameter for calculating the standard deviation of the input-referred offset voltage are given in Table 4.4.

Table 4.4: OTA input-referred offset parameters.

Symbol	Theoretical Value	Unit
$\sigma_{VT1}$	3.937	mV
$\sigma_{VT2}$	4.382	mV
$\sigma_{VT3}$	4.797	mV
$\sigma_{eta 1}$	0.8	%
$\sigma_{eta 2}$	0.9	%
$\sigma_{eta 3}$	1	%
$\xi_{VT}$	0.244	-
$\xi_{eta}$	3.961	-
$\sigma_{VT}^2$	19.291	$mV^2$
$\sigma_{VT}$	4.392	mV
$\sigma_{eta}^2$	0.4	$mV^2$
$\sigma_{eta}$	0.6	mV
$\sigma_{Vos}$	4.434	mV

From Table 4.4, we see that the  $\beta$ -mismatch is negligible and that the input-referred offset voltage is dominated by the contribution of the  $V_T$ -mismatch from the differential pair.

#### 4.4 Current and power consumption

The total current consumption, ignoring the current drawn by  $M_{5a}$ , is  $I_{tot} = (2 + A_1 + A_3) \cdot I_b$ . Assuming the input differential pait  $M_{1a}$ - $M_{1b}$  is biased in weak inversion, the bias current is directly related to the gain-bandwidth product GBW according to

$$I_b \cong nU_T \cdot \frac{C_L}{A_3} \cdot GBW.$$
 (4.12)

The minimum total current consumption can then be estimated as

$$I_{tot,min} \cong \frac{2 + A_1 + A_3}{A_3} \cdot nU_T \cdot C_L \cdot GBW. \tag{4.13}$$

The bias current and the total current are proportional to the gain-bandwidth product GBW and the load capacitance  $C_L$ . In the case  $A_1 = A_2 = A_3 = 1$ , we have

$$I_{tot,min} \cong 4 \cdot nU_T \cdot C_L \cdot GBW = 793 \ nA.$$

The actual current consumption accounting for some margin taken on the GBW is given by

 $I_{tot} = 4I_b = 1.12 \ \mu A$  which is 1.412 larger than the absolute minimum current consumption. This larger current consumption is mostly due to the parasitic capacitances at the output which add to the exsiting load capacitance and require a larger transconductance and hence a larger current to achive the same GBW.

The above design will now be checked against simulations.

## 5 Simulation results from ngspice

The theoretical results can be validated with the results obtained from simulations performed with ngspice. In order to run the simulations you need to have ngspice correctly installed. Please refer to the installation instructions.

#### Note

The simulations are performed with the PSP 103.6 compact model [7] using the parameters from the IHP open source PDK [5]. For ngspice, we use the Verilog-A implementation given in the IHP package [5] and compiled the OSDI file with OpenVAF [10] to run with ngspice [11]. In addition to the PSP user manual [7] a documentation of PSP and other MOSFET compact models and their parameter extraction can be found in [12].

#### 5.1 Operating point

We first write the parameter file for this specific design for running the ngspice simulations. Before running the AC and NOISE simulations, we first need to check the quiescent voltages and currents and the operating points of all transistors by running a .OP simulation.

Table 5.1: OTA node voltages with the OTA in open-loop without offset correction.

Node	Voltage
vdd	1.2
vb1	0.5
vb2	0.6
inp	0.6
$_{ m inn}$	0.6
out	0.379383
ic	0.6
$\operatorname{id}$	0
1	0.38783
2	0.618201
3	0.468461
4	0.618201
5	0.348266
6	0.88422
8	0.452642

From the node voltages shown in Table 5.1, we see that the output voltage  $V_{outq} = 379 \ mV$  is too low and is pushing  $M_7$  and  $M_{3b}$  out of saturation. This is due to the current mismatch in  $M_{2c}$  and  $M_{2d}$  and between  $M_{3a}$  and  $M_{3b}$  due to different drain voltages and finite output conductances leading to a different current flowing in  $M_{2d}$  and  $M_4$  compared to that flowing in  $M_{3b}$  and  $M_7$ . Even if the current difference is very small, it results in a large voltage debiasing at the output because of the high output resistance provided by the cascode stages.

Therefore simulating the open-loop gain for high gain amplifiers is not easy to perform without closing the loop. There are basically two approaches to simulate the open-loop gain for high-gain amplifiers:

- 1) Imposing a DC offset voltage to the amplifier in open-loop configuration that brings the output voltage back to normal (for example equal to the input common-mode voltage) or
- 2) Simulating the closed-loop gain (for example in voltage follower mode with a feedback gain of 1) and extracting the open-loop gain from the closed loop gain according to

$$A_{open-loop}(\omega) = \frac{A_{closed-loop}(\omega)}{1 - A_{closed-loop}(\omega)},$$
(5.1)

where  $A_{closed\text{-}loop}(\omega)$  is the simulated closed-loop transfer function and  $A_{open\text{-}loop}(\omega)$ , the computed open-loop transfer function. The above relation assumes that the open-loop DC gain is large enough for the input-referred offset voltage to be ignored.

The input-referred offset voltage can be extracted from the closed-loop voltage follower circuit as

$$V_{os} = V_{in} - \left(1 + \frac{1}{A}\right) \cdot V_{out} \cong V_{in} - V_{out} \quad \text{for } A \gg 1,$$

$$(5.2)$$

where  $A \triangleq A_{open-loop}(0)$  is the open-loop DC gain which can be assumed to be much larger than 1. This means that, provided the DC open-loop gain is sufficiently large, the offset voltage can be measured at the amplifier differential input after imposing the proper input common-mode voltage  $V_{ic}$ .

We can now simulate the OTA in closed-loop as a voltage follower.

Table 5.2: OTA node voltages with the OTA in voltage follower configuration.

Node	Voltage
vdd	1.2
vb1	0.5
vb2	0.6
inp	0.6
out	0.599885
1	0.387776
2	0.618382
3	0.468256
4	0.618022
5	0.368709
6	0.886269
8	0.452642

From the node voltages of the OTA in voltage follower configuration shown in Table 5.2, we see that now the output voltage  $V_{outq} = 600 \ mV$  is very close to the input voltage that has been set to  $V_{ic} = 600 \ mV$ . We can then extract the corresponding offset voltage  $V_{os} \cong V_{in} - V_{out} = 115.000 \ \mu V$ .

We can now apply this offset voltage to the open-loop operating point point simulation.

Table 5.3: OTA node voltages with the OTA in open-loop including offset correction.

Node	Voltage
vdd	1.2
vb1	0.5
vb2	0.6
inp	0.600058

Table 5.3: OTA node voltages with the OTA in open-loop including offset correction.

Node	Voltage
inn	0.599942
out	0.601797
ic	0.6
$\operatorname{id}$	0.000115
1	0.38783
2	0.618381
3	0.468256
4	0.61802
5	0.368788
6	0.886289
8	0.452642

From the node voltages of the OTA in open-loop configuration shown in Table 5.3 after adding the offset voltage at the input, we see that now the output voltage  $V_{outq} = 602 \ mV$  of the open-loop circuit is sufficiently close to the common-mode input voltage  $V_{ic} = 600 \ mV$ .

The operating point information for all transistors are extracted from the ngspice .op file. The data is split into the large-signal operating informations in Table 5.4, the small-signal operating point informations in Table 5.5 and the noise operating point informations in Table 5.6.

We can compare the results of the .op file (for example the inversion coefficient IC) to the results of the design given in Table 3.7. We observe that the values are close.

Similarly we can compare the small-signal parameters (for example the gate transconductance  $G_m$ ) resulting from the .op file to the results of the design presented in Table 3.8. Again, we see that they are reasonably close.

Table 5.4: Operating point information extracted from ngspice op file for each transistor.

Transistor	$I_D[nA]$	$V_{GS}$ $[mV]$	$V_{DS}$ $[mV]$	$V_{SB}$ $[mV]$	$V_{GS} - V_T [mV]$	$V_{Dsat} [mV]$
M1a	276.710	212	231	0	-57	111
M1b	277.486	212	230	0	-57	111
M2a	276.706	582	582	-0	241	227
M2b	277.482	582	582	-0	241	227
M2c	277.498	582	732	-0	241	227
M2d	274.522	582	314	-0	241	227
M3a	277.486	468	468	0	304	266
M3b	274.523	468	369	0	304	266
M4	274.520	386	284	314	-46	114
M5a	559.996	453	453	0	268	242
M5b	554.197	453	388	0	268	242
M7	274.520	231	233	369	-51	110

Table 5.5: PSP small-signal operating point information extracted from ngspice .op file for each transistor.

Transistor	$G_m \left[ \mu A/V \right]$	$G_{mb} \left[ \mu A/V \right]$	$G_{ds} [nA/V]$
M1a	7.946	1.106	384.145
M1b	7.966	1.109	385.327

Table 5.5: PSP small-signal operating point information extracted from ngspice .op file for each transistor.

Transistor	$G_m \left[ \mu A/V \right]$	$G_{mb} \left[ \mu A/V \right]$	$G_{ds} [nA/V]$
M2a	2.142	0.397	6.172
M2b	2.146	0.398	6.182
M2c	2.148	0.398	4.553
M2d	2.114	0.392	25.182
M3a	1.861	0.255	27.240
M3b	1.842	0.253	33.197
M4	7.570	1.210	94.539
M5a	4.187	0.569	85.211
M5b	4.148	0.564	94.234
M7	8.142	0.915	390.442

Table 5.6: PSP noise operating point information extracted from ngspice .op file for each transistor.

Transistor	$S_{ID,th} \left[ A^2/Hz \right]$	$S_{ID,fl}$ at 1Hz $[A^2/Hz]$
M1a	8.186e-26	6.210e-21
M1b	8.208e-26	6.246 e-21
M2a	5.166e-26	3.069e-21
M2b	5.175e-26	3.081e-21
M2c	5.181e-26	3.079e-21
M2d	5.138e-26	3.011e-21
M3a	2.330e-26	7.866e-22
M3b	2.307e-26	7.743e-22
M4	1.448e-25	4.286e-20
M5a	5.228e-26	9.943e-21
M5b	5.175e-26	9.795 e- 21
M7	8.192e-26	2.750e-21

Table 5.7: sEKV parameters calculated from the values extracted from the simulation.

Transistor	$W_{eff} [\mu m]$	$L_{eff} [\mu m]$	$W_{eff}/L_{eff}$	$I_{spec} [\mu A]$	$\overline{IC}$
M1a	2.540	0.581	4.371	3.096	0.089
M1b	2.540	0.581	4.371	3.096	0.090
M2a	0.310	3.876	0.080	0.020	14.143
M2b	0.310	3.876	0.080	0.020	14.183
M2c	0.310	3.876	0.080	0.020	14.183
M2d	0.310	3.876	0.080	0.020	14.031
M3a	0.170	7.181	0.024	0.017	16.549
M3b	0.170	7.181	0.024	0.017	16.372
M4	2.830	0.283	9.996	2.445	0.112
M5a	0.170	2.731	0.062	0.044	12.702
M5b	0.170	2.731	0.062	0.044	12.570
M7	3.970	0.941	4.218	2.988	0.092

Table 5.8: sEKV small-signal parameters calculated from the values extracted from the simulation.

Transistor	$G_{spec} \left[ \mu A/V \right]$	n	$G_m \left[ \mu A/V \right]$	$G_{ms} \left[ \mu A/V \right]$	$G_{ds} [nA/V]$
M1a	119.687	1.139	7.946	9.052	384.145
M1b	119.687	1.139	7.966	9.075	385.327
M2a	0.756	1.185	2.142	2.539	6.172
M2b	0.756	1.185	2.146	2.543	6.182
M2c	0.756	1.185	2.148	2.546	4.553
M2d	0.756	1.186	2.114	2.506	25.182
M3a	0.648	1.137	1.861	2.116	27.240
M3b	0.648	1.137	1.842	2.095	33.197
M4	94.532	1.160	7.570	8.780	94.539
M5a	1.705	1.136	4.187	4.756	85.211
M5b	1.705	1.136	4.148	4.712	94.234
M7	115.514	1.112	8.142	9.057	390.442

Table 5.9: sEKV noise parameters calculated from the values extracted from the simulation.

Transistor	$\sqrt{S_{nin,th}} \left[ nV/\sqrt{Hz} \right]$	$R_{nin,th} [k\Omega]$	$\gamma_n [-]$	$\sqrt{S_{nin,fl}} \left[ nV/\sqrt{Hz} \right]$
M1a	36.008	78.219	0.622	9917.558
M1b	35.963	78.026	0.622	9920.670
M2a	106.087	678.955	1.455	25857.765
M2b	106.011	677.987	1.455	25867.833
M2c	105.968	677.440	1.455	25833.396
M2d	107.239	693.788	1.466	25962.182
M3a	82.035	405.988	0.756	15071.439
M3b	82.448	410.085	0.755	15105.685
M4	50.266	152.427	1.154	27347.997
M5a	54.611	179.919	0.753	23815.915
M5b	54.848	181.486	0.753	23862.711
M7	35.153	74.551	0.607	6440.649

We can also check the bias voltages and operating region of each transistor which are given in Table 5.10.

Table 5.10: Bias voltages and operating regions extracted from ngspice for each transistor.

Trans.	Type	Funct.	$V_G[V]$	$V_S[V]$	$V_D[V]$	$V_{DS}$ $[mV]$	$V_{DSsat} [mV]$	Reg.	Sat.
M1a	n	DP	0.212	0.000	0.231	231	111	WI	sat
M1b	n	DP	0.212	0.000	0.230	230	111	WI	sat
M2a	p	CM	0.582	0.000	0.582	582	227	$\operatorname{SI}$	$\operatorname{sat}$
M2b	p	CM	0.582	0.000	0.582	582	227	$\operatorname{SI}$	sat
M2c	p	CM	0.582	0.000	0.732	732	227	$\operatorname{SI}$	$\operatorname{sat}$
M2d	p	CM	0.314	0.000	0.314	314	227	$\operatorname{SI}$	sat
M3a	$\mathbf{n}$	CM	0.468	0.000	0.468	468	266	$\operatorname{SI}$	sat
M3b	$\mathbf{n}$	CM	0.468	0.000	0.369	369	266	$\operatorname{SI}$	sat
M4	p	CA	0.700	0.314	0.598	284	114	MI	sat
M5a	$\mathbf{n}$	CM	0.453	0.000	0.453	453	242	$\operatorname{SI}$	sat
M5b	$\mathbf{n}$	CM	0.453	0.000	0.388	388	242	$\operatorname{SI}$	$\operatorname{sat}$
M7	p	CA	0.600	0.369	0.602	233	110	WI	sat

From Table 5.10, we see that all transistors are biased in saturation. The operating points look fine. We can now proceed with the simulation of the open-loop large-signal transfer characteristic.

#### 5.2 Large-signal differential transfer characteristic

We now simulate the DC differential transfer characteristic. We can then check the systematic offset voltage that was extracted above. The simulation of the large-signal input-output characteristic is presented in Figure 5.1.

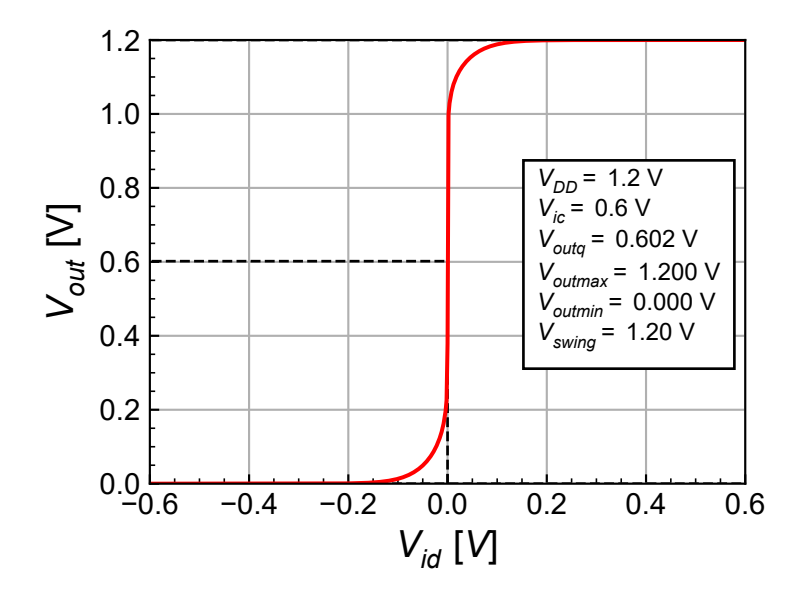


Figure 5.1: Simulated large-signal input-output characteristic.

We can now zoom into the high gain region in order to extract a more accurate value of the offset voltage and the output swing. The simulation results are presented in Figure 5.2.

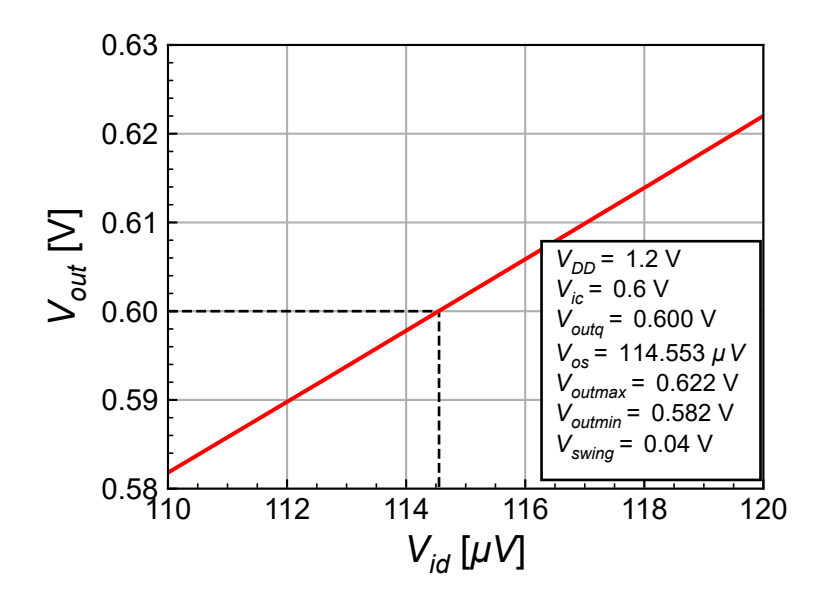


Figure 5.2: Zoom of the simulated large-signal input-output characteristic in the gain region.

We can now save a more accurate value of the offset voltage  $V_{os}=114.553~\mu V$  that is required to bring the output voltage to  $V_{ic}=600~mV$  and that will be used for the following .AC and .NOISE simulations.

#### 5.3 Open-loop gain

#### 5.3.1 Closed-loop circuit

As explained above we can extract the open-loop gain from the simulated closed-loop gain with the amplifier operating as a voltage follower. The open-loop gain is then given by

$$A_{open-loop}(\omega) = \frac{A_{closed-loop}(\omega)}{1 - A_{closed-loop}(\omega)},$$
(5.3)

where  $A_{closed\text{-}loop}(\omega)$  is the simulated closed-loop transfer function and  $A_{open\text{-}loop}(\omega)$ , the computed open-loop transfer function. The above relation assumes that the open-loop DC gain is large enough for the input-referred offset voltage to be ignored.

Note that we need to have a sufficient number of digits for the simulated closed-loop gain because the latter is very close to 1. The simulations results are shown in Figure 5.3.

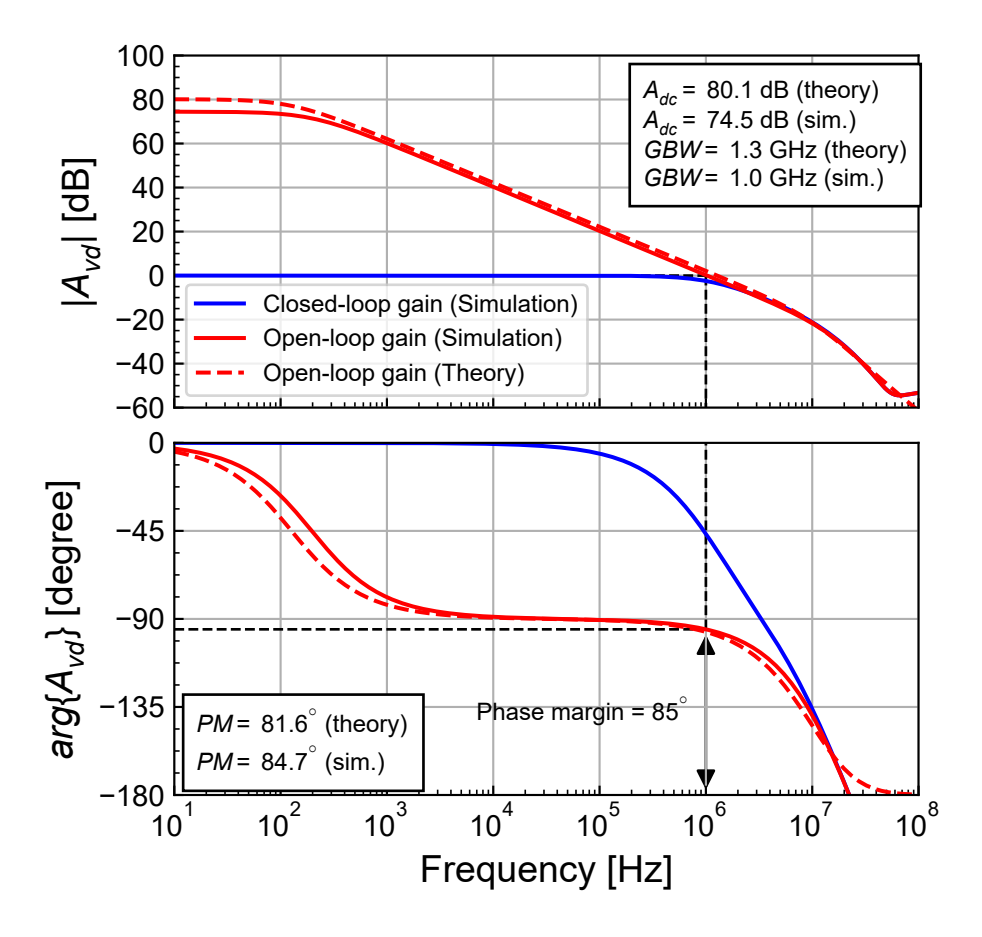


Figure 5.3: Open-loop gain response extracted from the closed-loop simulations and compared to theoretical estimation.

From Figure 5.3, we see that the simulated GBW is right on target but slightly smaller than the estimated value. The simulated DC gain is much smaller than the theoretical estimation but slightly above spec. We can now simulate the open-loop gain directly in open-loop configuration and compare the results to those achieved from the closed-loop simulation.

#### 5.3.2 Open-loop circuit

After having checked the operating point information, extracted the offset voltage and making sure that the OTA output is not saturated, we can now proceed with the open-loop gain simulation. The simulation results are presented in Figure 5.4.

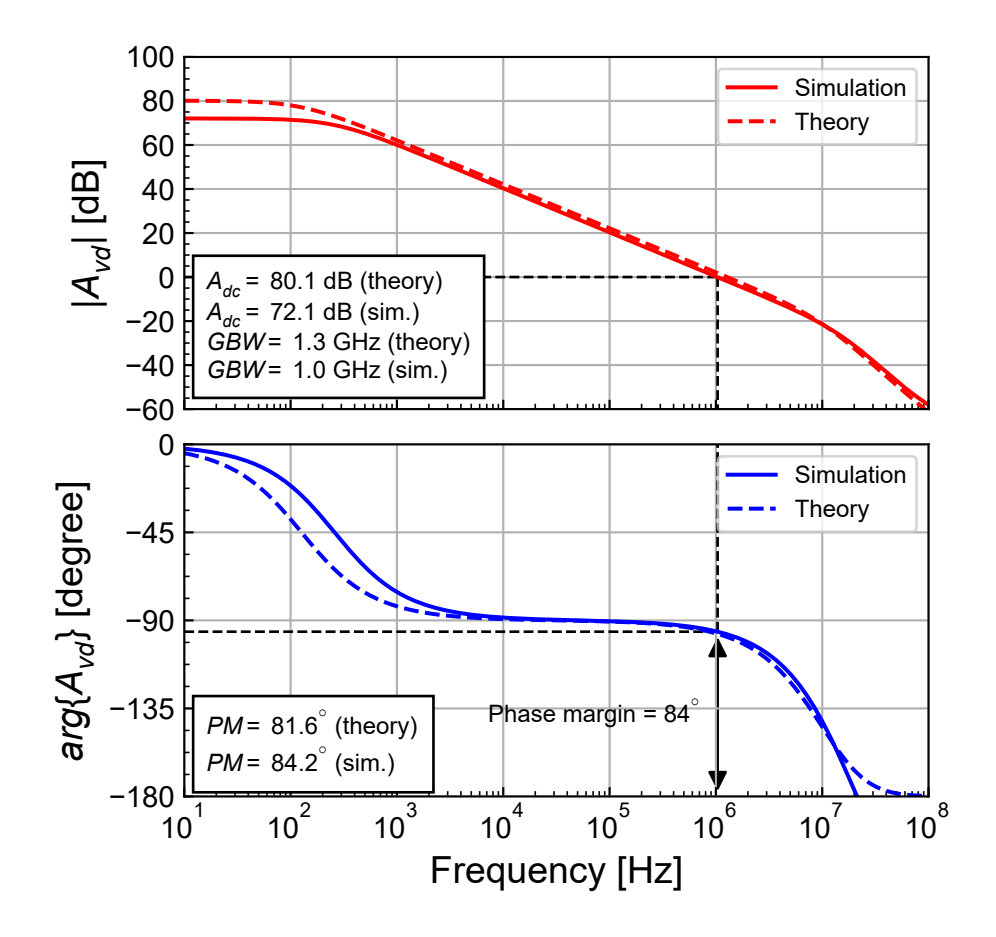


Figure 5.4: Simulated gain response compared to theoretical estimation.

The results of the open-loop simulation in Figure 5.4 are very close to the result extracted from the closed-loop simulation except at high frequency (above the GBW frequency). The GBW is the same than the value extracted from the closed-loop simulation, smaller than the estimated one but still on target. The DC gain obtained from the open-loop simulation gain is slightly smaller than the value extracted from the closed-loop simulation and much smaller than the theoretical estimation, but still within spec. The low value of the DC gain is due to the high output conductance of nMOS transitors in this technology, while the difference between simulation and theoretical prediction is due to the poor output conductance model that is used in the design phase.

#### 5.4 Input-referred noise

The simulated input-referred noise PSD is presented in Figure 5.5 and compared to the theoretical estimation.

From Figure 5.5, we see that the simulated input-referred noise PSD is larger than the theoretical estimation for both flicker and white noise. We can have a closer look at the contributions of the various transistors to the input-referred white noise PSD.

The contributions of  $M_{1a}$ - $M_{1b}$ ,  $M_{2a}$ - $M_{2b}$ - $M_{2c}$ - $M_{2d}$ ,  $M_{3a}$ - $M_{3b}$  and the cascode transistors  $M_4$  and  $M_7$  to the input-referred white noise PSD are detailed in Figure 5.6 and compared to the theoretical white noise. We can observe that the white noise is dominated by the differential pair  $M_{1a}$ - $M_{1b}$  while the contribution of  $M_{2a}$ - $M_{2b}$ - $M_{2c}$ - $M_{2d}$  and  $M_{3a}$ - $M_{3b}$  are lower. We also see that the contribution of the cascode transistors is more than 50 dB lower and can therefore be neglected. The total simulated white noise is slightly higher than the theoretical estimation, which is acceptable. This results in an OTA thermal noise excess factor  $\gamma_{n,ota} = 3.849$  that is slightly larger than the predicted value  $\gamma_{n,ota} = 2.407$ .

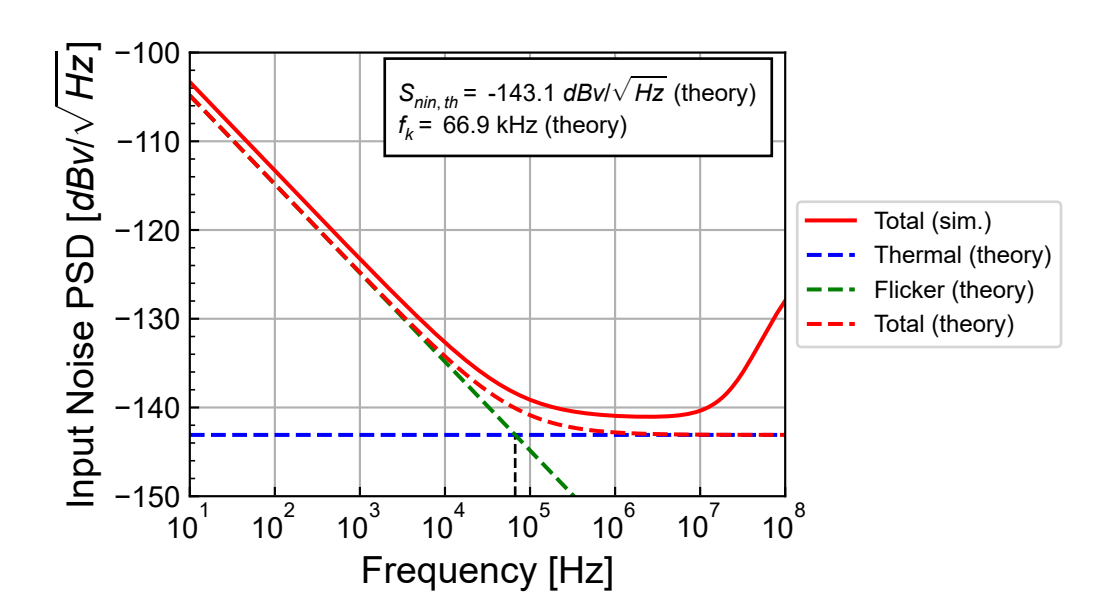


Figure 5.5: Simulated input-referred noise PSD compared to theoretical estimation.

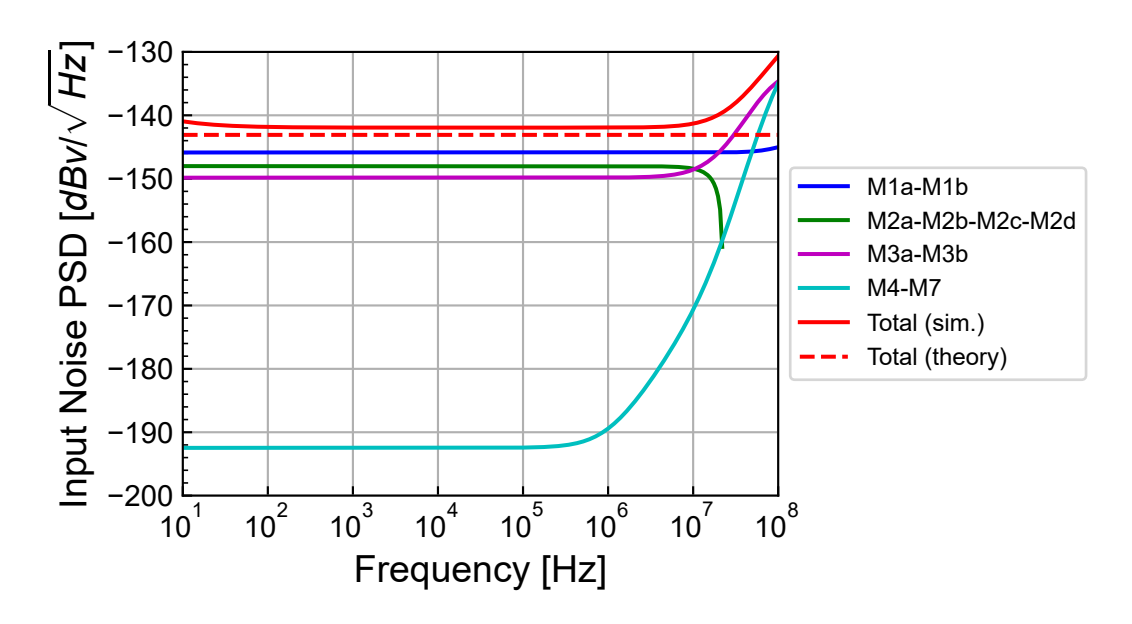


Figure 5.6: Breakdown of the contributions to the simulated input-referred white noise PSD.

Figure 5.7 presents the breakdown of the contributions of the various transistors to the input-referred flicker noise. As expected from the design,  $M_{2a}$ - $M_{2b}$ - $M_{2c}$ - $M_{2d}$  contribute about the same than  $M_{1a}$ - $M_{1b}$ .

The breakdown of the contributions of the various transistors to the total input-referred noise is presented in Figure 5.7. We can observe that the simulation is slightly larger than the theoretical estimation.

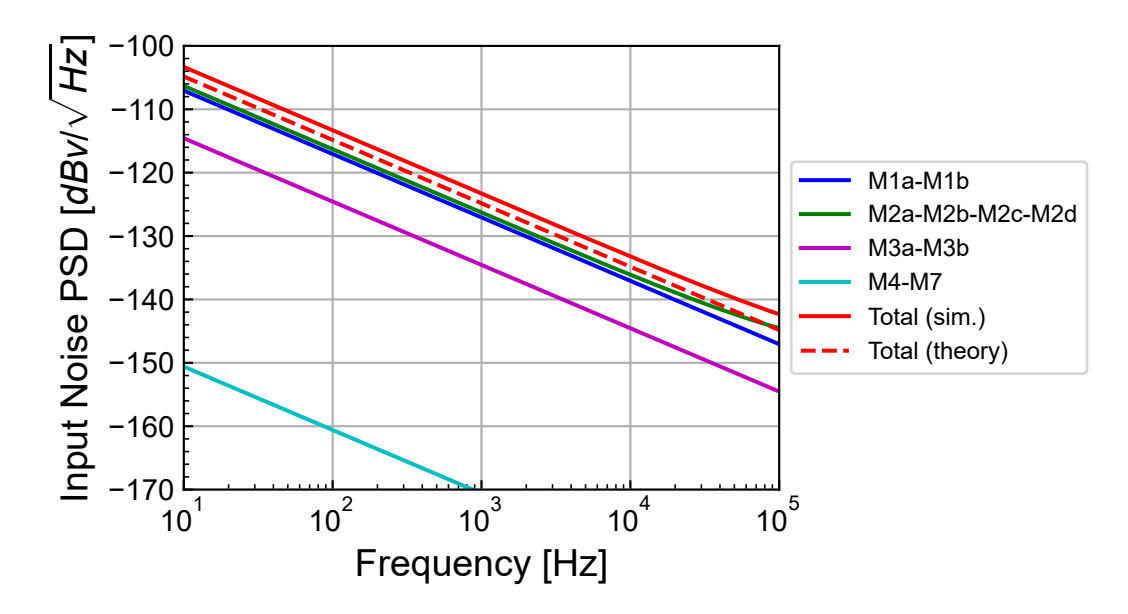


Figure 5.7: Breakdown of the contributions to the simulated input-referred flicker noise PSD.

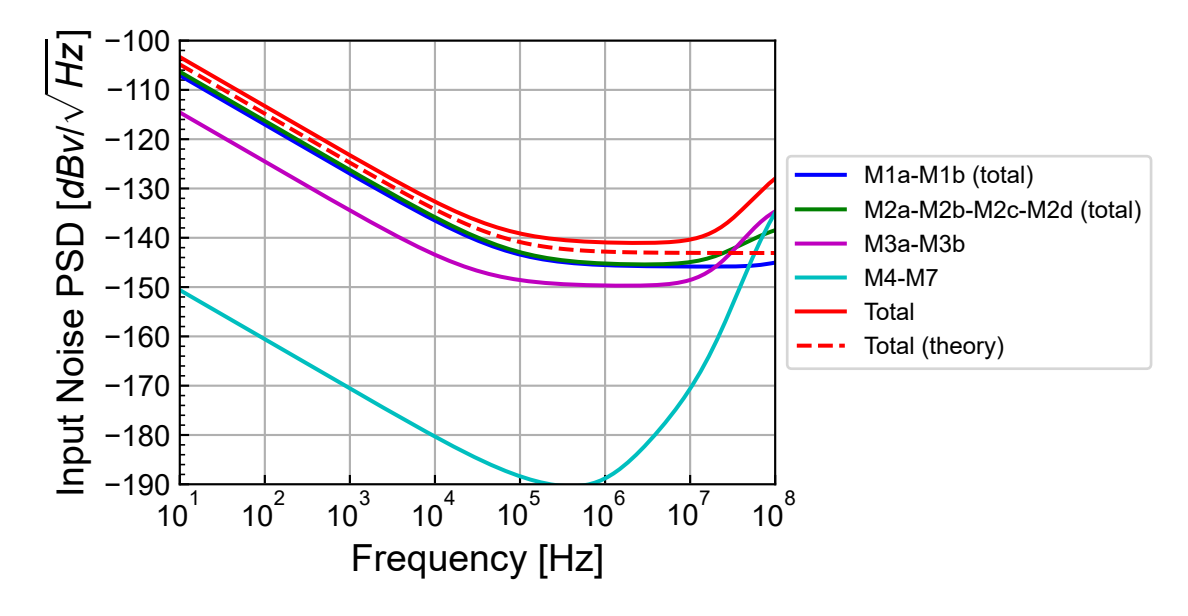


Figure 5.8: Breakdown of the contributions to the simulated input-referred noise PSD.

### 5.5 Input common-mode voltage range

We can check the input common-mode voltage range by connecting the OTA as a voltage follower and sweeping the positive input. As shown in Figure 5.9, the output follows the input voltage up to  $0.9\,V$ . So the input common-mode voltage range is about  $0.9\,V$ .

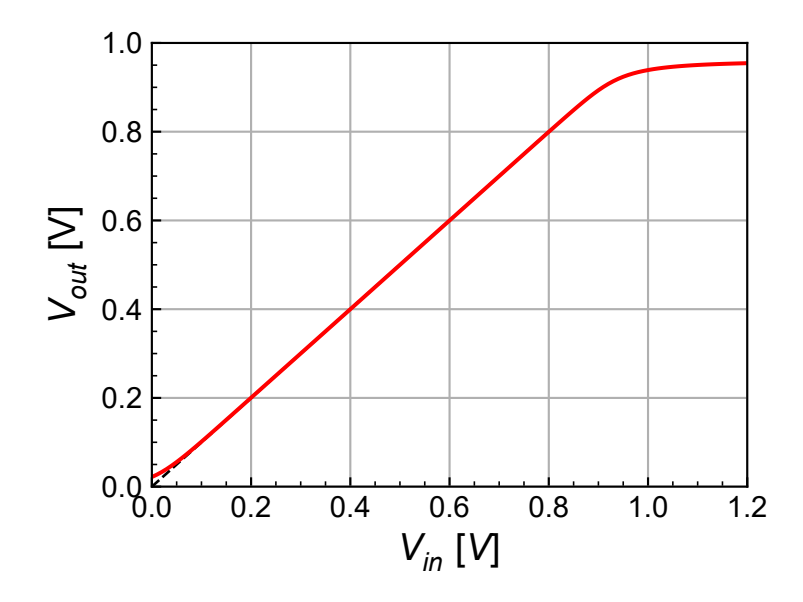


Figure 5.9: Simulated input common-mode voltage range.

#### 5.6 Step-response

In this section we will check the step response of the OTA operating as a voltage follower (output connected to the negative input) with the same load capacitance  $C_L = 1 \ pF$ . According to the input common-mode voltage range established above, we will set the input common-mode voltage to  $V_{ic} = 0.3 \ V$  to leave enough room for the large step.

#### 5.6.1 Small-step

We start by imposing a small step  $\Delta V_{in} = 10~mV$  on top of a common mode voltage  $V_{ic} = 0.3~V$ . The simulation results are shown in Figure 5.10 where  $\Delta V_{in}(t) \triangleq V_{in+}(t) - V_{ic}$  and  $\Delta V_{out}(t) \triangleq V_{out}(t) - V_{outq}$  with  $V_{outq} \cong V_{ic}$  is the quiescent output voltage.  $\Delta V_{in}$  and  $\Delta V_{out}$  are compared to the response of a single pole circuit having a cut-off frequency equal to the GBW. The difference between the simulation and the first-order model is due to the larger estimated value of the GBW and the additional poles introduced by the current mirrors.

#### 5.6.2 Large step

We now impose a larger step  $\Delta V_{in} = 300~mV$  on top of a common mode voltage  $V_{ic} = 300~mV$ . The simulation results are shown in Figure 5.11 where  $\Delta V_{in}(t) \triangleq V_{in+}(t) - V_{ic}$  and  $\Delta V_{out}(t) \triangleq V_{out}(t) - V_{outq}$  with  $V_{outq} \cong V_{ic}$  is the quiescent output voltage.  $\Delta V_{in}$  and  $\Delta V_{out}$  are compared to the response of a single pole circuit having a cut-off frequency equal to the GBW. We now observe the effect of slew-rate which increases the settling time.

## 5.7 Current and power consumption

The total current consumption (without accounting for the current in  $M_{5a}$ ) is given by  $I_{tot} = 1.120$   $\mu A$ , resulting in a total power consumption given by  $P = 1.344~\mu W$ . We can compare the current and power consumption of the Miller OTA to the telescopic OTA  $I_{tot,telescopic} \cong 0.5~\mu A$ . The current and power consumption of the symmetrical cascode OTA is 2.240 times larger than that of the telescopic OTA for the same specifications and performance.

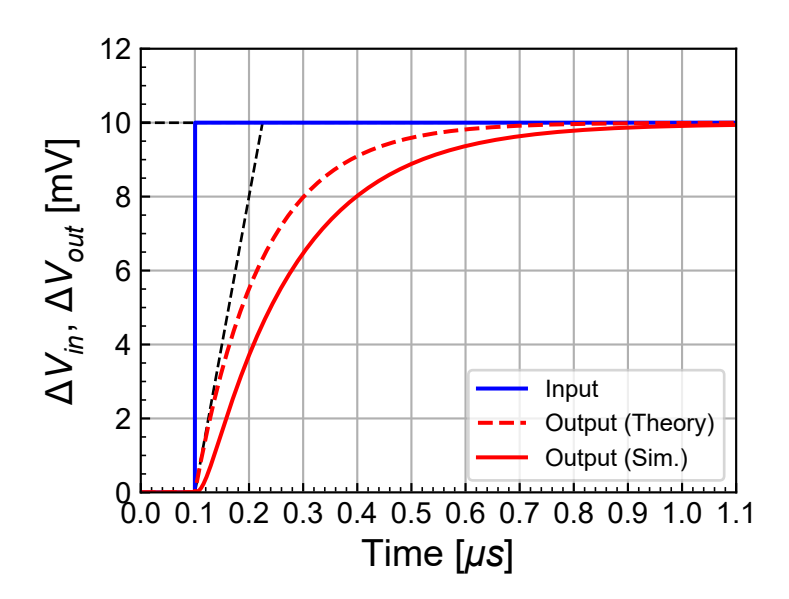


Figure 5.10: Step response of the OTA as a voltage follower for a small input step.

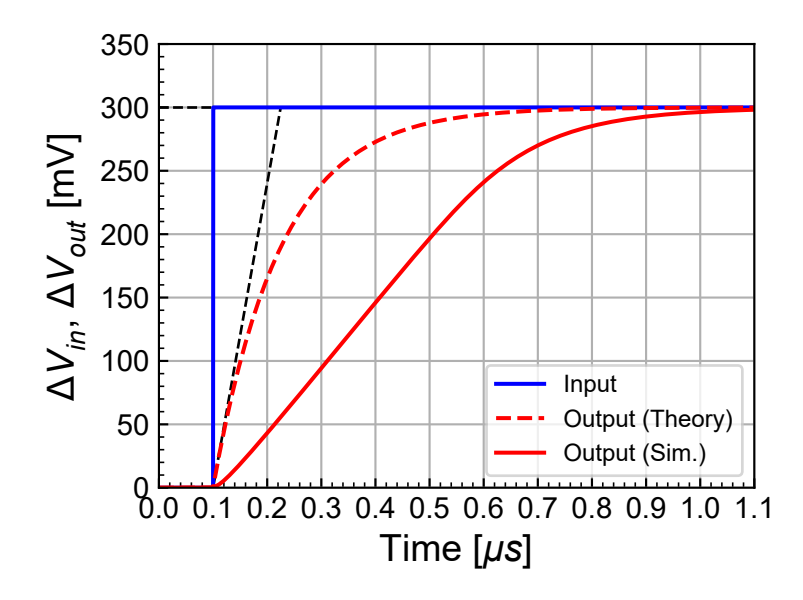


Figure 5.11: Step response of the OTA as a voltage follower for a large input step highlighting the slew-rate effect.

## 6 Conclusion

This notebook presented the detailed analysis, design and verification by simulation of the symmetrical OTA [1]. The analysis allowed to derive the design equations to achieve the target specifications. The OTA has been designed for specifications on the gain-bandwidth product and DC gain in the IHP SG13G2 130nm BiCMOS technology [5] using the inversion coefficient approach with the sEKV model and parameters [2] [3] [4]. The design has been validated by simulations with the ngspice simulator [6] using the PSP compact model [7] and the parameters provided by the open source IHP [5]. The simulations have shown that the gain-bandwidth and DC gain specifications are achieved despite the limited intrinsic gain of nMOS transistors of this technology.

## References

- [1] F. Krummenacher, "High voltage gain CMOS OTA for micropower SC filters," *Electronics Letters*, vol. 17, no. 4, pp. 160–162, 1981.
- [2] C. C. Enz and E. A. Vittoz, Charge-Based MOS Transistor Modeling The EKV Model for Low-Power and RF IC Design, 1st ed. John Wiley, 2006.
- [3] C. Enz, F. Chicco, and A. Pezzotta, "Nanoscale MOSFET Modeling: Part 1: The Simplified EKV Model for the Design of Low-Power Analog Circuits," *IEEE Solid-State Circuits Magazine*, vol. 9, no. 3, pp. 26–35, 2017.
- [4] C. Enz, F. Chicco, and A. Pezzotta, "Nanoscale MOSFET Modeling: Part 2: Using the Inversion Coefficient as the Primary Design Parameter," *IEEE Solid-State Circuits Magazine*, vol. 9, no. 4, pp. 73–81, 2017.
- [5] IHP, "IHP SG13G2 Open Source PDK." https://github.com/IHP-GmbH/IHP-Open-PDK, 2025.
- [6] Holger Vogt, Giles Atkinson, Paolo Nenzi, "Ngspice User's Manual Version 43." https://ngspice.sourceforge.io/docs/ngspice-43-manual.pdf, 2024.
- [7] G.D.J. Smit, A.J. Scholten, D.B.M. Klaassen, O. Rozeau, S. Martinie, T. Poiroux and J.C. Barbé, "PSP 103.6 The PSP model is a joint development of CEA-Leti and NXP Semiconductors." https://www.cea.fr/cea-tech/leti/pspsupport/Documents/psp103p6\_summary.pdf, 2017.
- [8] F. Krummenacher, E. Vittoz, and M. Degrauwe, "Class AB CMOS amplifier micropower SC filters," *Electronics Letters*, vol. 17, no. 13, pp. 433–435, 1981.
- [9] M. G. Degrauwe, J. Rijmenants, E. A. Vittoz, and H. J. D. Man, "Adaptive biasing CMOS amplifiers," *IEEE Journal of Solid-State Circuits*, vol. 17, no. 3, pp. 522–528, 1982.
- [10] SemiMod GmbH, "Open VAF." https://openvaf.semimod.de/docs/getting-started/introduction/, 2025.
- [11] Dietmar Warning, "Verilog-A Models for Circuit Simulation." https://github.com/dwarning/VA-Models, 2024.
- [12] Agilent Technologies, "IC-CAP 2008, Nonlinear Device Models Volume 1." https://people.ece .ubc.ca/robertor/Links\_files/Files/ICCAP-2008-doc/pdf/icmdl.pdf, 2008.